

Off-shell effects in Higgs processes at a linear collider and implications for the LHC

Stefan Liebler^a, Gudrid Moortgat-Pick^{a,b}, Georg Weiglein^a

^a *DESY, Notkestraße 85,
22607 Hamburg, Germany*

^b *II. Institut für Theoretische Physik, Universität Hamburg,
Luruper Chaussee 149
22761 Hamburg, Germany*

Abstract

The importance of off-shell contributions is discussed for $H \rightarrow VV^{(*)}$ with $V \in \{Z, W\}$ for large invariant masses m_{VV} involving a standard model (SM)-like Higgs boson with $m_H = 125 \text{ GeV}$ at a linear collider (LC). Both dominant production processes $e^+e^- \rightarrow ZH \rightarrow ZVV^{(*)}$ and $e^+e^- \rightarrow \nu\bar{\nu}H \rightarrow \nu\bar{\nu}VV^{(*)}$ are taken into account, and the signal processes are compared with background yielding the same final state. The relative size of the off-shell contributions is strongly dependent on the centre-of-mass energy. These contributions can have an important impact on the determination of cross sections and branching ratios. However, the combination of on- and off-shell contributions can also be utilised to lift degeneracies allowing to test higher-dimensional operators, unitarity and light and heavy Higgs interferences in extended Higgs sectors. The latter is demonstrated in the context of a 2-Higgs-Doublet model. We also discuss the impact of these aspects for the Large Hadron Collider (LHC) where they are relevant. The importance of a precise measurement of the Higgs mass for on-shell contributions in $H \rightarrow VV^{(*)}$ is emphasized. A particular focus is put on methods for extracting the Higgs width at a LC. Off-shell contributions are shown to have a negligible impact on the width determination at low \sqrt{s} when applying the Z recoil method to extract branching ratios in combination with an appropriate determination of a partial width. On the other hand, off-shell contributions can be exploited to constrain the Higgs width in a similar fashion as in recent analyses at the LHC. It is demonstrated that this approach, besides relying heavily on theoretical assumptions, is affected by the negative interference of Higgs and background contributions that may limit the sensitivity that is achievable with the highest foreseeable statistics at the LHC and a LC.

e-mail addresses:

stefan.liebler@desy.de, gudrid.moortgat-pick@desy.de, georg.weiglein@desy.de

1 Introduction

With the spectacular discovery of a signal in the Higgs searches at the Large Hadron Collider (LHC) [1, 2] particle physics entered a new era. Detailed measurements of the mass, spin and CP properties of the new particle, its couplings to the other standard model (SM) particles, its total width and its self-coupling will be crucial to reveal the underlying mechanism of electroweak symmetry breaking. The determination of significant deviations from the properties predicted in the SM would have profound implications in this context, indicating for instance the presence of additional states of an extended Higgs sector or a composite nature of the observed state. The required high-precision measurements will have to be complemented with sufficiently accurate theory predictions for the observables accessible with current and future experimental data.

A special role in this endeavour will be played by a future linear e^+e^- collider like the International Linear Collider (ILC), for which a detailed technical design report [3–8] exists. In contrast to the LHC a linear e^+e^- collider will not only improve significantly the precision on the Higgs couplings to the SM gauge bosons and fermions, but moreover will provide a model-independent measurement of the width of the Higgs boson. For a SM Higgs boson of $m_H = 125 \text{ GeV}$ the latter is tiny, namely just $\Gamma_H^{\text{SM}} = 4.07 \text{ MeV}$ [9–11]. Since the width is orders of magnitude below the detector resolution of high-energy physics experiments, an access to it by a measurement of the differential distribution with respect to the invariant mass of the decay products is impossible.

Recently off-shell contributions in $H \rightarrow VV^{(*)}$ with $V \in \{Z, W\}$ at the LHC attracted significant attention. The term “off-shell” refers to contributions where the invariant mass m_{VV} of the two gauge bosons exceeds the Higgs mass, $m_{VV} \gg m_H$. A recent discussion of the off-shell contributions for the dominant LHC production process can be found in Refs. [12–15], earlier works on Higgs boson contributions to $gg \rightarrow \gamma\gamma/VV$ in Refs. [16–18]. It is remarkable that in combination with on-shell contributions – but relying heavily on theoretical assumptions – the off-shell contributions can be used to constrain the Higgs width [19]. Meanwhile the theoretical knowledge with respect to higher orders and jet vetoes was significantly improved for various final states in Refs. [20–26]. An experimental analysis was recently presented by the CMS collaboration quoting an upper bound of $4.2 \cdot \Gamma_H^{\text{SM}}$ on the Higgs boson width [27, 28]. The ATLAS collaboration obtained a bound of $(4.8 - 7.7) \cdot \Gamma_H^{\text{SM}}$ [29]. Moreover off-shell decays of a Higgs boson can be utilised to put constraints on higher-dimensional operators, as worked out for the LHC in Refs. [30, 31]. Refs. [32–34] elaborate on the extraction of the top Yukawa coupling from the resolution to long- and short-distance contributions to Higgs production via gluon fusion.

In this work we want to investigate the off-shell effects in $H \rightarrow VV^{(*)}$ for a linear collider in different regimes of the centre-of-mass (cms) energy and as a function of the polarisation of the initial state. In contrast to gluon fusion at the LHC the main production mechanisms at an e^+e^- collider occur already at tree-level, namely Higgsstrahlung, where the Higgs is radiated of a Z boson, and vector-boson-fusion (VBF), where the Higgs stems from the fusion of two weak gauge bosons. The discussion of off-shell effects in $H \rightarrow VV^{(*)}$ is closely related to the inadequacy of the zero-width approximation (ZWA) for the two production processes. We quantify the size of the off-shell effects for both processes and analyse their significance with respect to the background yielding the same final state. Based on those results the impact of off-shell contributions is discussed in various contexts:

- ▷ Depending on the cms energy we investigate their influence on the measurements of cross sections and branching ratios and on the determination of Higgs-boson properties that can be inferred from those measurements. The impact of the off-shell contributions on the extraction of Higgs couplings at low cms energies \sqrt{s} , i.e. close to the production threshold, is small. At high \sqrt{s} , on the other hand, their influence increases, and they can be utilised to test higher-dimensional operators and to check the destructive interference between Higgs and background contributions at high invariant masses m_{VV} . In extended Higgs sectors light and heavy Higgs contributions can interfere over a large range of m_{VV} , which we demonstrate in the context of a 2-Higgs-Doublet model (2HDM).
- ▷ We show the importance of a precise Higgs mass measurement for the on-shell Higgs contributions in $H \rightarrow VV^{(*)}$, whereas off-shell contributions are mostly insensitive to the precise numerical value of the Higgs mass.
- ▷ We also discuss off-shell contributions in the context of the Higgs width determination at a linear collider. The state-of-the-art method is based on the detection of the Z decay products in Higgsstrahlung (Z recoil method) yielding an absolute measurement of Higgs branching ratios in combination with an appropriate determination of a partial width. With this procedure the Higgs width can be determined in a model-independent way, see Refs. [35–39], and a high precision for the Higgs width is achieved. This method is affected by off-shell effects for low cms energies only at the sub-permil level. Bounding the Higgs width from the combination of on-shell and off-shell contributions, on the other hand, is mainly limited by the destructive interference of Higgs and background contributions.

For quantitative statements we use `MadGraph5_aMC@NLO` [40] to simulate the full processes $e^+e^- \rightarrow 6$ fermions. In our discussion we also address the choice of the Higgs propagator, the inclusion of initial state radiation and beamstrahlung, as well as higher order contributions.

The outline of the paper is as follows: In Section 2 we start our discussion with a short description of the Higgs propagator structure. Then we quantify off-shell contributions in $e^+e^- \rightarrow ZH$ and $e^+e^- \rightarrow \nu\bar{\nu}H$ followed by $H \rightarrow ZZ^{(*)}$ and $H \rightarrow W^\pm W^\mp^{(*)}$ in Section 3. The issue of gauge dependence is discussed in this context. The off-shell contributions are quantified with respect to the on-shell ones and with respect to the background. Of particular importance is the mainly destructive interference between Higgs induced contributions and the background. We investigate different cms energies and the dependence on the polarisation of the initial state, as well as the dependence on the precise numerical value of the Higgs mass. In Section 4 we address the impact on the Z recoil method and the extraction of Higgs to gauge boson couplings at an e^+e^- collider. After a brief discussion of the tests of unitarity and the sensitivity to higher-dimensional operators we subsequently describe the two processes $e^+e^- \rightarrow \nu\bar{\nu} + 4$ jets and $e^+e^- \rightarrow \mu^+\mu^- + 4$ jets and their dependence on Higgs induced contributions in Section 5. We discuss the inclusion of initial state radiation and beamstrahlung as well as higher order effects in Section 6. The latter should be taken into account in future analyses. We then investigate the sensitivity of the two above example processes on the Higgs width in Section 7 and comment on the limitations of the method in case of the LHC. Finally we discuss the interference of an on-shell heavy Higgs with the off-shell light Higgs contributions in the context of a 2-Higgs-Doublet model in Section 8. We conclude in Section 9.

2 Relation of the Higgs mass and width to the complex pole of the propagator

Before we start our discussion of off-shell effects in $H \rightarrow VV^{(*)}$ in the subsequent section, we shortly elaborate on the relation between the mass and total width of the Higgs boson and the complex pole of the propagator. Denoting with m_0 the tree-level Higgs mass and with $\hat{\Sigma}$ the renormalized self-energy of the Higgs propagator, the complex pole is obtained through the relation $\mathcal{M}^2 - m_0^2 + \hat{\Sigma}(\mathcal{M}^2) = 0$, where the complex pole can be written in the form $\mathcal{M}^2 = m_H^2 - im_H\Gamma_H$. Therein m_H is the physical Higgs mass and Γ_H the total width of the Higgs boson. Expanding the inverse propagator around the complex pole yields

$$p^2 - m_0^2 + \hat{\Sigma}(p^2) \simeq (p^2 - \mathcal{M}^2) \left\{ 1 + \hat{\Sigma}'(\mathcal{M}^2) \right\} \quad (1)$$

in the vicinity of the complex pole. Accordingly, the Higgs propagator in the vicinity of the complex pole can be expressed in the well-known form of a Breit-Wigner propagator with constant width Γ_H ,

$$\Delta_H(p^2) = \frac{i}{p^2 - \mathcal{M}^2} = \frac{i}{p^2 - m_H^2 + im_H\Gamma_H}. \quad (2)$$

Away from the pole, i.e. in the far off-shell region with $p^2 \gg m_H^2$, the Higgs width is not of relevance. For the specific processes that are considered in this paper our choice is equivalent to the complex-mass scheme [41, 42], which is known to provide gauge-independent results. Differences with respect to the scheme defined in Refs. [43–45] are expected to be small, in particular since the constant width Γ_H is close to the width therein [45]. For our subsequent discussion we fix $m_H = 125 \text{ GeV}$ and $\Gamma_H^{\text{SM}} = 4.07 \cdot 10^{-3} \text{ GeV}$, the latter in accordance with the prescription of the LHC Higgs cross section working group (LHC-HXSWG) [9–11].

3 Off-shell contributions in $H \rightarrow ZZ^{(*)}$ and $H \rightarrow W^\pm W^\mp^{(*)}$

Given the two dominant production processes for a Higgs boson H at a linear collider, $e^+e^- \rightarrow ZH$ and $e^+e^- \rightarrow \nu\bar{\nu}H$, we discuss the validity of the zero-width approximation (ZWA) for the Higgs decays $H \rightarrow WW^{(*)}$ and $H \rightarrow ZZ^{(*)}$ within this section. The relevant Feynman diagrams are presented in Fig. 1. Our discussion follows Refs. [12–14], which are specific to the dominant production process at the LHC, gluon fusion.

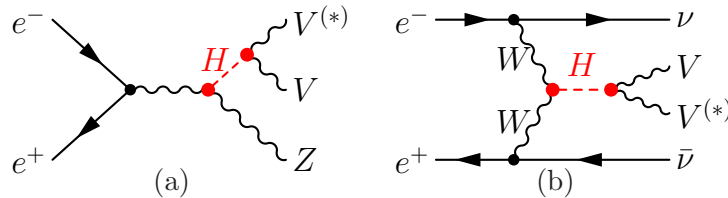


Figure 1: Feynman diagrams for (a) $e^+e^- \rightarrow ZH \rightarrow ZVV^{(*)}$; (b) $e^+e^- \rightarrow \nu\bar{\nu}H \rightarrow \nu\bar{\nu}VV^{(*)}$.

Supplementing the ZWA for the production and the decay part of the process with a Breit-Wigner propagator, the differential cross section $e^+e^- \rightarrow ZH \rightarrow ZVV$ can be written

as (see e.g. Ref. [12])

$$\left(\frac{d\sigma_{\text{ZWA}}^{ZVV}}{dm_{VV}}\right) = \sigma^{ZH}(m_H) \frac{2m_{VV}}{(m_{VV}^2 - m_H^2)^2 + (m_H\Gamma_H)^2} \frac{m_H\Gamma_{H\rightarrow VV}(m_H)}{\pi}, \quad (3)$$

with $m_{VV}^2 = p_H^2$ being the invariant mass of the two gauge bosons originating from the intermediate Higgs H . The production cross sections $e^+e^- \rightarrow ZH$ is represented by σ^{ZH} , the partial width of an on-shell Higgs boson into two gauge bosons by $\Gamma_{H\rightarrow VV}(m_H)$, given in the restframe of the Higgs boson H . Integrating over the invariant mass m_{VV} in the limit where $m_H\Gamma_H \rightarrow 0$ results in the well-known formula

$$\sigma_{\text{ZWA}}^{ZVV} = \sigma^{ZH}(m_H) \frac{\Gamma_{H\rightarrow VV}(m_H)}{\Gamma_H} = \sigma^{ZH}(m_H) \text{BR}_{H\rightarrow VV}(m_H). \quad (4)$$

Going beyond the ZWA, one can define (see e.g. Ref. [12]) an off-shell production cross section according to

$$\left(\frac{d\sigma_{\text{off}}^{ZVV}}{dm_{VV}}\right) = \sigma^{ZH}(m_{VV}) \frac{2m_{VV}}{(m_{VV}^2 - m_H^2)^2 + (m_H\Gamma_H)^2} \frac{m_{VV}\Gamma_{H\rightarrow VV}(m_{VV})}{\pi}. \quad (5)$$

The result is identical to the explicit calculation of the Higgs induced production cross section $e^+e^- \rightarrow ZH \rightarrow ZVV$ with $m_{VV} > 2m_V$ at tree-level. The formulas can be directly translated to the production process $e^+e^- \rightarrow \nu\bar{\nu}H \rightarrow \nu\bar{\nu}VV$. Our own code, generated with **FeynArts** [46, 47] and **FormCalc** [48], makes use of the 't Hooft-Feynman-gauge and explicitly takes into account Goldstone boson contributions. **MadGraph5_aMC@NLO** [40] by default uses unitary gauge, allowing us to check the gauge independence. For the considered case of lowest order in perturbation theory within the SM the choice of all diagrams involving a Higgs is gauge independent, since the Goldstone bosons do not couple to the initial state (in good approximation the electron and positron can be treated as massless). The dependence on the Higgs mass m_H , which is an independent parameter of the SM, is suppressed for high invariant masses of the two gauge bosons m_{VV} . The leading (Higgs-mass independent) contributions for high m_{VV} cancel with the corresponding background contributions involving gauge bosons, as it is required in order to restore unitarity for the scattering of longitudinally polarised gauge bosons.

Two processes need particular attention: For $e^+e^- \rightarrow \nu\bar{\nu}W^+W^-$ we present the result just involving the s -channel Higgs boson in the off-shell region corresponding to the approximation of Eq. (5), $e^+e^- \rightarrow \nu\bar{\nu}H \rightarrow \nu\bar{\nu}W^+W^-$. In a second step we add the contribution induced by t -channel Higgs boson exchange between the two gauge bosons, see Fig. 2.

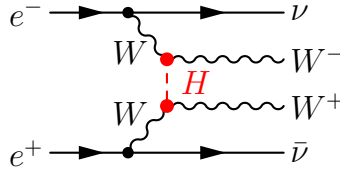


Figure 2: t -channel Feynman diagram for $e^+e^- \rightarrow \nu\bar{\nu}W^+W^-$.

In case of $e^+e^- \rightarrow ZH \rightarrow ZZZ$ it is at first sight unclear which two out of the three Z bosons originate from a Higgs boson. For the most conservative approach we average over the

three possible invariant mass combinations m_{ZZ} . If only one out of the two gauge bosons to calculate the invariant mass m_{ZZ} stems from the Higgs boson, the invariant mass m_{ZZ} cannot be related to the on/off-shellness of the Higgs boson, and contributions with an on-shell Higgs boson enter the differential cross section over a wide range of values of m_{ZZ} , also in the region $m_{ZZ} > 2m_Z$. Necessarily the peak in the on-shell region $m_{ZZ} \approx m_H$ is mainly induced by contributions with the correct assignment of the two gauge bosons to the Higgs boson and thus the averaging over the three invariant mass combinations approximately corresponds to a division of the cross section obtained by Eq. (5) by a factor of 3. For $m_{ZZ} > 2m_Z$ all assignments of ZZ pairs are of relevance and interferences between the three possible options need to be taken into account, which we calculate separately by our code. Taking the average of possible ZZ pairings effectively increases the relevance of the off-shell contributions with respect to the on-shell region for this specific process due to the possibly “wrong” assignment of gauge bosons, which as mentioned already causes on-shell Higgs events to contribute in the region $m_{ZZ} > 2m_Z$. In a more optimistic approach, using different weights for the ZZ pairings a discrimination between the different ZZ pairs could be achieved. In our notation the latter case is indicated by additional indices, $e^+e^- \rightarrow Z_1Z_2Z_3$, in order to emphasize the distinction of the Z bosons. To summarise, for $e^+e^- \rightarrow \nu\bar{\nu}H \rightarrow \nu\bar{\nu}W^+W^-$ and $e^+e^- \rightarrow Z_1H \rightarrow Z_1Z_2Z_3$ we do not only present the results obtained by the usage of Eq. (5), but also add results obtained by taking into account t -channel contributions and averaging over the different ZZ pairs, $e^+e^- \rightarrow ZH \rightarrow ZZZ$, respectively. Lastly we note that the final states $e^+e^- \rightarrow \nu\bar{\nu}VV$ can also be obtained via $e^+e^- \rightarrow ZH \rightarrow \nu\bar{\nu}VV$. However, Higgsstrahlung is sub-dominant in regions where vector boson fusion is of relevance and can be moreover suppressed by appropriate cuts. It is thus addressed in the background discussion, see Section 3.2.

When using Eq. (5) we calculate the production cross sections σ^{ZH} and $\sigma^{\nu\bar{\nu}H}$ using our own code and obtain the partial width $\Gamma_{H \rightarrow VV}$ from the values for the branching ratio $\text{BR}_{H \rightarrow VV}$ and the Higgs width Γ_H given by the LHC-HXSWG [9–11]. For $m_{VV} > 2m_V$ the partial width $\Gamma_{H \rightarrow VV}$ is rather close to the tree-level partial width, which enters our explicit calculation of production cross sections.

The resulting differential cross sections $d\sigma/dm_{ZZ}$ for both production processes in combination with $H \rightarrow ZZ^{(*)}$ for different energies $\sqrt{s} = 250, 350, 500 \text{ GeV}$ and 1 TeV and a fixed polarisation of the initial state $\text{Pol}(e^+, e^-) = (0.3, -0.8)$ are shown in Fig. 3. For $e^+e^- \rightarrow ZZZ$ we distinguish the pure usage of Eq. (5), $e^+e^- \rightarrow Z_1H \rightarrow Z_1Z_2Z_3$, from the case with averaging over the three possible invariant mass combinations of ZZ pairs, $e^+e^- \rightarrow ZH \rightarrow ZZZ$, the latter presented by the red, dot-dashed curve. As expected the average over the three ZZ pairs results in a larger off-shell cross section due to on-shell Higgs events which contribute also in the region $m_{ZZ} > 2m_Z$. Similarly, Fig. 4 shows the differential cross sections for $H \rightarrow WW^{(*)}$, where for $e^+e^- \rightarrow \nu\bar{\nu}WW$ the red, dot-dashed curve includes also the t -channel Higgs induced contributions. For $m_{VV} > 2m_V$ we add the contributions from background diagrams leading to the same final state as blue curve in both Fig. 3 and Fig. 4. The full process $e^+e^- \rightarrow ZZZ$ includes all signal and background Feynman diagrams and thus averaging over the three ZZ pairs is obsolete. A detailed description of the background is provided in Section 3.2. For $m_{VV} < 2m_V$ only resonant background processes are of relevance. Thus in case of $H \rightarrow WW^{(*)}$ the Z boson peak at $m_{WW} \approx m_Z$ is present, but not visible in our diagrams which start at $m_{WW} = 100 \text{ GeV}$.

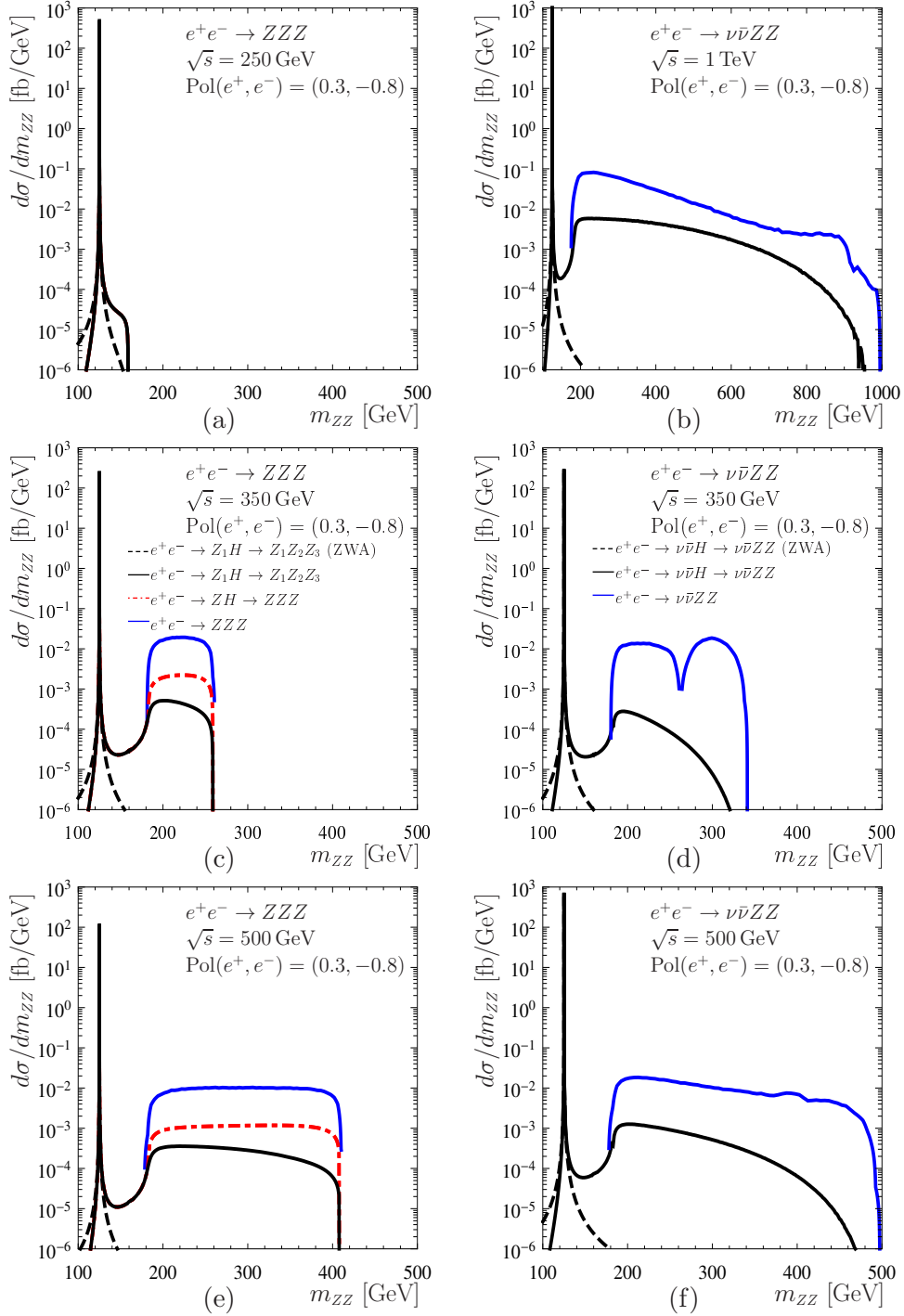


Figure 3: $d\sigma/dm_{ZZ}$ in fb/GeV as a function of m_{ZZ} in GeV defined in Eq. (3) (ZWA) (black, dashed) and Eq. (5) (black, solid) for a fixed polarisation $\text{Pol}(e^+, e^-) = (0.3, -0.8)$ for (a,c,e) $e^+e^- \rightarrow Z_1H \rightarrow Z_1Z_2Z_3$ for cms energies $\sqrt{s} = 250, 350, 500$ GeV (top to bottom) and (b,d,f) $e^+e^- \rightarrow \nu\bar{\nu}H \rightarrow \nu\bar{\nu}ZZ$ for cms energies $\sqrt{s} = 1000, 350, 500$ GeV (top to bottom). The black curves in (a,c,e) are shown as a function of $m_{Z_2Z_3}$. The red, dot-dashed curve shows the calculation of $e^+e^- \rightarrow ZH \rightarrow ZZZ$ with averaging over the ZZ pairs. As blue curve we add the complete calculation including background contributions $e^+e^- \rightarrow ZZZ/\nu\bar{\nu}ZZ$, see Section 3.2. The legend of the centered figures is valid for the upper and lower figures as well.

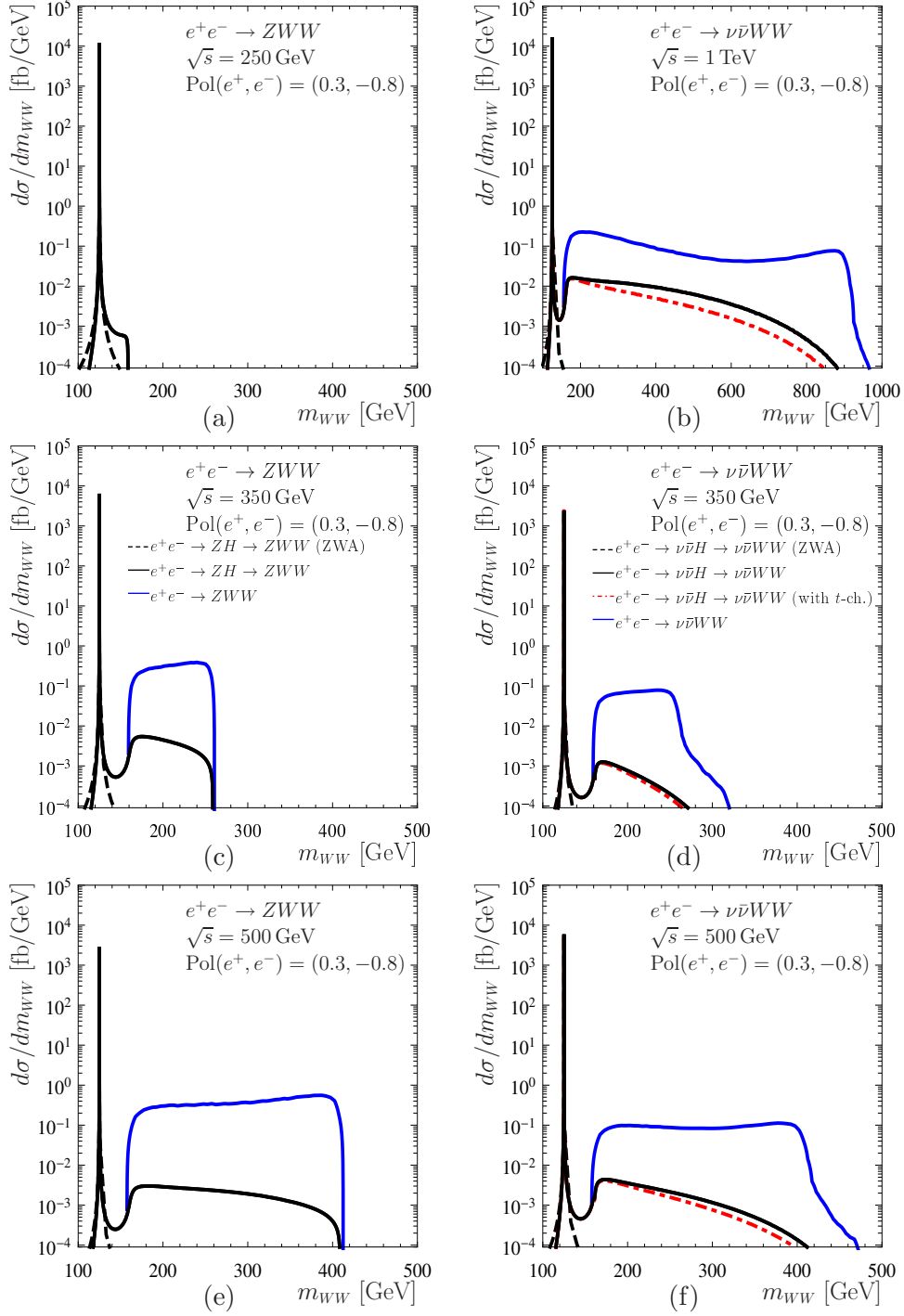


Figure 4: $d\sigma/dm_{WW}$ in fb/GeV as a function of m_{WW} in GeV defined in Eq. (3) (ZWA) (black, dashed) and Eq. (5) (black, solid) for a fixed polarisation $\text{Pol}(e^+, e^-) = (0.3, -0.8)$ for (a,c,e) $e^+e^- \rightarrow ZH \rightarrow ZWW$ for cms energies $\sqrt{s} = 250, 350, 500$ GeV (top to bottom) and (b,d,f) $e^+e^- \rightarrow \nu\bar{\nu}H \rightarrow \nu\bar{\nu}WW$ for cms energies $\sqrt{s} = 1000, 350, 500$ GeV (top to bottom). The red, dot-dashed curve shows the calculation of $e^+e^- \rightarrow \nu\bar{\nu}WW$ including s- and t-channel Higgs induced contributions, see text. As blue curve we add the complete calculation including background contributions $e^+e^- \rightarrow ZWW/\nu\bar{\nu}WW$, see Section 3.2. The legend of the centered figures is valid for the upper and lower figures as well.

Given the inclusive cross section for a lower and upper bound of invariant masses m_{VV}

$$\sigma_X(m_{VV}^d, m_{VV}^u) = \int_{m_{VV}^d}^{m_{VV}^u} dm_{VV} \left(\frac{d\sigma_X}{dm_{VV}} \right) \quad (6)$$

we define the relative importance of the off-shell signal contributions in the form

$$\Delta_{\text{off}}^{ZVV} = \frac{\sigma_{\text{off}}^{ZVV}(130\text{GeV}, \sqrt{s} - m_Z)}{\sigma_{\text{off}}^{ZVV}} \quad \text{and} \quad \Delta_{\text{off}}^{\nu\bar{\nu}VV} = \frac{\sigma_{\text{off}}^{\nu\bar{\nu}VV}(130\text{GeV}, \sqrt{s})}{\sigma_{\text{off}}^{\nu\bar{\nu}VV}} \quad , \quad (7)$$

with $\sigma_{\text{off}}^{ZVV} = \sigma_{\text{off}}^{ZVV}(0, \sqrt{s} - m_Z)$ and $\sigma_{\text{off}}^{\nu\bar{\nu}VV} = \sigma_{\text{off}}^{\nu\bar{\nu}VV}(0, \sqrt{s})$. Our discussion is hardly sensitive to the precise numerical value of the boundary between on- and off-shell contributions, which we choose to be at 130 GeV. In contrast to the absolute size of the off-shell contributions, their relative size Δ_{off} is independent of the polarisation of the initial state electron/positron. As a function of the cms energy the latter values are given in Tab. 1.

\sqrt{s}	$\sigma_{\text{off}}^{Z_1 Z_2 Z_3} (\sigma_{\text{off}}^{ZZZ})$	$\Delta_{\text{off}}^{Z_1 Z_2 Z_3} (\Delta_{\text{off}}^{ZZZ})$	$\sigma_{\text{off}}^{\nu\bar{\nu}ZZ}$	$\Delta_{\text{off}}^{\nu\bar{\nu}ZZ}$
250 GeV	3.12(3.12) fb	0.03(0.03) %	0.490 fb	0.12 %
300 GeV	2.36(2.40) fb	0.46(1.83) %	1.12 fb	0.40 %
350 GeV	1.71(1.82) fb	1.82(7.77) %	1.91 fb	0.88 %
500 GeV	0.802(0.981) fb	7.20(24.1) %	4.78 fb	2.96 %
1 TeV	0.242(0.341) fb	30.9(50.9) %	15.0 fb	13.0 %
\sqrt{s}	$\sigma_{\text{off}}^{ZWW}$	$\Delta_{\text{off}}^{ZWW}$	$\sigma_{\text{off}}^{\nu\bar{\nu}WW}$	$\Delta_{\text{off}}^{\nu\bar{\nu}WW}$
250 GeV	76.3 fb	0.03 %	3.98(3.99) fb	0.13(0.12) %
300 GeV	57.7 fb	0.42 %	9.07(9.08) fb	0.29(0.26) %
350 GeV	41.4 fb	0.92 %	15.5(15.5) fb	0.49(0.43) %
500 GeV	18.6 fb	2.61 %	38.2(38.1) fb	1.21(0.96) %
1 TeV	4.58 fb	11.0 %	110.8(108.9) fb	4.45(2.78) %

Table 1: Inclusive cross sections $\sigma_{\text{off}}(0, \sqrt{s} - m_Z)$ for $e^+e^- \rightarrow ZH \rightarrow ZVV$ and $\sigma_{\text{off}}(0, \sqrt{s})$ for $e^+e^- \rightarrow \nu\bar{\nu}H \rightarrow \nu\bar{\nu}VV$ for $\text{Pol}(e^+, e^-) = (0.3, -0.8)$ and relative size of the off-shell contributions Δ_{off} in %. In brackets we add the results averaging over the ZZ pairs for $e^+e^- \rightarrow ZZZ$ and taking into account the t -channel Higgs contribution for $e^+e^- \rightarrow \nu\bar{\nu}WW$. Δ_{off} is independent of the polarisation.

The off-shell contributions are sizeable and reach $\mathcal{O}(10\%)$ for large enough cms energies. For $H \rightarrow WW^{(*)}$ the off-shell contributions are generally smaller than for $H \rightarrow ZZ^{(*)}$, since the difference between $\Gamma_{H \rightarrow WW}(m_H)$ and $\Gamma_{H \rightarrow WW}(2m_W)$ is not as pronounced as for $H \rightarrow ZZ^{(*)}$. On the other hand the off-shell contributions are very small for low cms energies, $\sqrt{s} = 250 - 300$ GeV. As a consequence, the determination of the HVV couplings based on the ZWA in that energy range is to a good approximation not affected by off-shell contributions. For the case of $H \rightarrow ZZ^{(*)}$ followed by decays of the two gauge bosons into leptons or quarks, i.e. $Z \rightarrow l^\pm l^\mp / q\bar{q}$, on-shell and off-shell contributions can be discriminated by the invariant mass of the four leptons/quarks. This is not necessarily the case when neutrinos are involved in the final state like e.g. in $H \rightarrow WW^{(*)}$ followed by $W \rightarrow l^\pm \nu(\bar{\nu})$, since the four particle invariant mass is not directly accessible, possibly only indirectly e.g. by the recoil mass in $e^+e^- \rightarrow ZH$. We discuss the implications for the Z recoil mass measurement and the extraction of HVV couplings in more detail in Section 4.1.

As a final step of this discussion we investigate the quality of the ZWA in the “on-shell” region between $(m_{VV}^d, m_{VV}^u) = (120, 130)$ GeV for $H \rightarrow VV^{(*)}$ by comparing $\sigma_{\text{ZWA}}(m_{VV}^d, m_{VV}^u)$ as defined in Eq. (3) with $\sigma_{\text{off}}(m_{VV}^d, m_{VV}^u)$ defined in Eq. (5). Within the specified interval the agreement between the cross sections is at the permil level, and most of the contribution stems from the small interval $m_{VV} = 124 - 126$ GeV. However, as soon as larger invariant masses $m_{VV} > 130$ GeV are taken into account the difference between both methods becomes visible in the plots of Fig. 3 and Fig. 4. Lower invariant masses in the range $(m_{VV}^d, m_{VV}^u) = (100, 120)$ GeV, on the other hand, are negligible. The difference between the two inclusive cross sections σ_{ZWA} and σ_{off} in the “on-shell region” is slightly increasing with the cms energy, but always stays at the permil level. We conclude that within the “on-shell region” the ZWA is a valid approximation with an accuracy at the (sub-)permil level.¹

3.1 Dependence on the precise numerical value of the Higgs mass

Both partial widths $\Gamma_{H \rightarrow ZZ}(m_H)$ and $\Gamma_{H \rightarrow WW}(m_H)$ and accordingly both branching ratios $\text{BR}_{H \rightarrow VV}(m_H)$ are strongly sensitive to the precise numerical value of the Higgs mass m_H for $m_H < 2m_V$. As an example, if the Higgs mass $m_H = 125$ GeV is changed by ± 200 MeV, both partial widths change by about $\pm 2.5\%$. Due to the dominance of $H \rightarrow b\bar{b}$ at $m_H = 125$ GeV the change in the total width is smaller and amounts to $\pm 0.7\%$. In order to briefly illustrate these effects we calculate uncertainties on the cross section using $m_H = 124.8 - 125.2$ GeV together with $\Gamma_H^{\text{SM}} = 4.04 - 4.10$ MeV for $\sqrt{s} = 500$ GeV with a fixed polarisation $\text{Pol}(e^+, e^-) = (0.3, -0.8)$ and present the results in Tab. 2.

$e^+e^- \rightarrow$	$\sigma_{\text{off}}(m_H)$	$\sigma_{\text{off}}(m_H \pm 200 \text{ MeV})$	$\delta\sigma_{\text{off}}$	Δ_{off}
$Z_1 Z_2 Z_3$ (ZZZ)	0.802 fb (0.981 fb)	0.788 – 0.816 fb (0.967 – 0.995 fb)	−1.7, +1.7% (−1.4, +1.4%)	7.31 – 7.10% (24.4 – 23.8)%
ZWW	18.66 fb	18.33 – 18.90 fb	−1.7, +1.3%	2.65 – 2.58%
$\nu\bar{\nu}ZZ$	4.78 fb	4.70 – 4.85 fb	−1.6, +1.6%	3.00 – 2.92%
$\nu\bar{\nu}WW$	38.16 fb (38.09 fb)	37.53 – 38.60 fb (37.46 – 38.53 fb)	−1.7, +1.2% (−1.7, +1.2%)	1.22 – 1.20% (0.957 – 0.973%)

Table 2: Cross sections σ_{off} (defined as in Tab. 1) and their dependence on the Higgs mass $m_H \pm 200$ MeV for $\sqrt{s} = 500$ GeV with a fixed polarisation $\text{Pol}(e^+, e^-) = (0.3, -0.8)$. $\delta\sigma_{\text{off}}$ shows the variation with respect to the central value. Δ_{off} shows the relevance of the off-shell contributions. In brackets we add the results averaging over the ZZ pairs for $e^+e^- \rightarrow ZZZ$ and taking into account the t -channel Higgs contribution for $e^+e^- \rightarrow \nu\bar{\nu}WW$.

The change is mainly induced in the on-shell region between $m_{VV} = 120 - 130$ GeV, whereas the off-shell contributions $m_{VV} > 130$ GeV only change at the sub-permil level. Thus, the relative fraction of the off-shell contributions, Δ_{off} , changes due to the effect in the on-shell region. Since Δ_{off} is inversely proportional to the on-shell contributions, the increase in the central value of the cross section by e.g. $\delta\sigma_{\text{off}} = 1\%$ with increasing Higgs mass m_H translates into a (relative) decrease of the off-shell contributions Δ_{off} by about $\mathcal{O}(1\%)$. The values provided in brackets again average over the three ZZ pairs for $e^+e^- \rightarrow ZZZ$

¹Our investigation here has been done for partonic cross sections. In an experimental simulation the definition of the “on-shell region” may have to be adjusted in order to take into account effects like detector resolution.

and take into account the t -channel Higgs contributions for $e^+e^- \rightarrow \nu\bar{\nu}WW$. For practical purposes the relative variation $\delta\sigma_{\text{off}}$ can be scaled linearly in order to investigate the case of higher accuracies in the Higgs mass, e.g. for $m_H \pm 50$ MeV $\delta\sigma_{\text{off}}(e^+e^- \rightarrow ZWW)$ is given by $-0.4, +0.3\%$. Due to the main effect in the on-shell region the variations $\delta\sigma_{\text{off}}$ are of similar size for different \sqrt{s} .

We conclude that the measurement of the Higgs mass to a precision below 100 MeV is of crucial importance to enable cross section predictions at the percent level for processes where the Higgs boson decays to weak gauge bosons. The strong dependence of the Higgs decay into weak gauge bosons on the Higgs mass has the consequence that any uncertainty in the Higgs mass translates into an uncertainty in the extraction of the couplings g_{HVV} from the observation of the decay products. In contrast, the coupling determination g_{HVV} from production processes followed by decays $H \rightarrow b\bar{b}$ or $\gamma\gamma$ is less sensitive to the Higgs mass. On the other hand the argument can also be turned around: the off-shell contributions in $H \rightarrow VV^{(*)}$ are not very sensitive to the Higgs mass value m_H . The different dependence of on- and off-shell contributions on the Higgs mass and width can be exploited in various ways, as will be discussed for some examples below.

3.2 Background contributions to $e^+e^- \rightarrow ZVV$ and $e^+e^- \rightarrow \nu\bar{\nu}VV$

In order to estimate the quality of a measurement of the Higgs induced off-shell contributions (named signal S in the following), for $m_{VV} > 2m_V$ a background (B) calculation as well as the interference (I) of the signal with the background for large invariant masses m_{VV} is needed. For low invariant masses $m_{VV} < 2m_V$ only resonant diagrams are of relevance, which are either the signal diagrams through the Higgs at $m_{VV} \approx m_H$ or possibly a Z boson peak at $m_{WW} \approx m_Z$, the latter for the WW final state only. The different types of Feynman diagrams for $e^+e^- \rightarrow ZVV$ are depicted in Fig. 5. For $e^+e^- \rightarrow \nu\bar{\nu}VV$ we will not list all types of diagrams. Few examples are shown in Fig. 6, more diagrams can be directly constructed from Fig. 5 by adding $Z \rightarrow \nu\bar{\nu}$. All neutrino flavours have to be taken into account for the background.

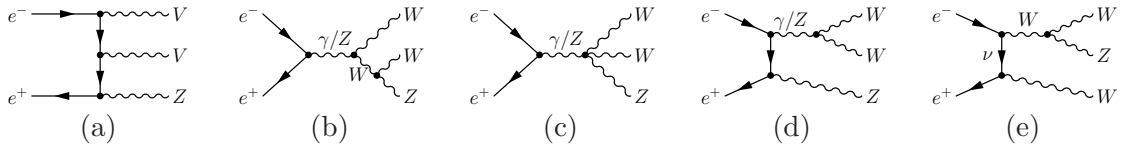


Figure 5: Example background diagrams $e^+e^- \rightarrow ZZZ$ and $e^+e^- \rightarrow ZWW$ with $V = W, Z$.

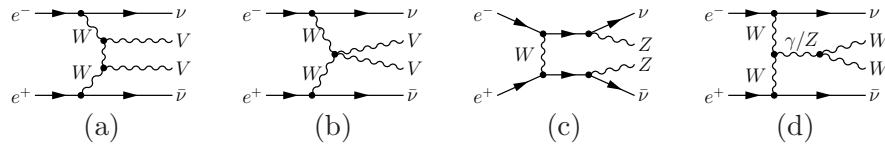


Figure 6: Example background diagrams $e^+e^- \rightarrow \nu\bar{\nu}ZZ$ and $e^+e^- \rightarrow \nu\bar{\nu}WW$ with $V = W, Z$.

In Fig. 3 above we display apart from the Higgs induced contributions S in black also the sum of all contributions $S+B+I$ (blue) for $e^+e^- \rightarrow ZZZ/\nu\bar{\nu}ZZ$. The sum of all contributions is obtained by `MadGraph5_aMC@NLO` [40] and extracted as a function of m_{VV} with the help

of `MadAnalysis` [49]. For the process $e^+e^- \rightarrow ZZZ$ we have also calculated the separate contributions S , B and I with our own code and found agreement at the permil level with the `MadGraph5_aMC@NLO` result. The background prediction for this process is in accordance with Ref. [50]. Fig. 4 provides the corresponding result for $e^+e^- \rightarrow ZWW/\nu\bar{\nu}WW$. For $e^+e^- \rightarrow ZWW/\nu\bar{\nu}WW/\nu\bar{\nu}ZZ$ the interference term I gives a negative contribution. The destructive interference is of particular importance for the process $e^+e^- \rightarrow \nu\bar{\nu} + 4\text{jets}$, see Section 5, and the sensitivity to the Higgs width in the off-shell region, see Section 7. The destructive interference between signal and background in this process is in fact closely related to the preservation of unitarity in scattering of longitudinal gauge bosons. For $e^+e^- \rightarrow ZZZ$, however, the interference term provides a positive contribution for all cms energies and the initial state polarisations as shown in Fig. 7. The relevant background diagram shown in Fig. 5 (a) only includes couplings of the Z bosons to fermions, but no couplings of weak gauge bosons among themselves. Accordingly, the background induced by the diagram Fig. 5 (a) is by itself not increasing with the cms energy. In case of $e^+e^- \rightarrow ZZZ$ the result after averaging over the ZZ pairs is understood as signal S . Fig. 7 additionally shows that the maximal cross section for $e^+e^- \rightarrow ZZZ$ is obtained for the polarisation $\text{Pol}(e^+, e^-) = (1.0, -1.0)$, however a suppression of the background and thus the signal-background interference with respect to the signal contribution can be obtained for $\text{Pol}(e^+, e^-) = (-1.0, 1.0)$.

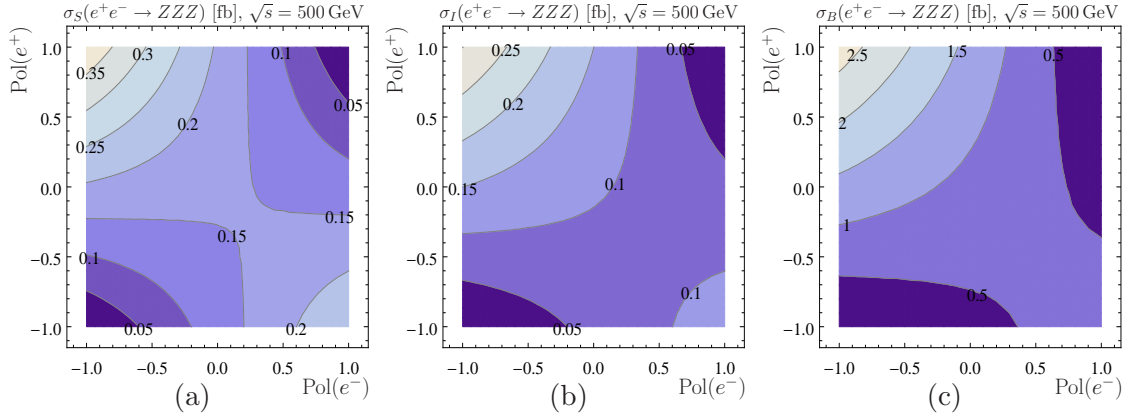


Figure 7: $\sigma(2m_V, \sqrt{s} - m_V)$ in fb for $e^+e^- \rightarrow ZZZ$ as a function of the polarisation of the initial state for $\sqrt{s} = 500$ GeV shown separately for (a) the signal contribution S ; (b) the signal-background interference I and (c) the background contribution B .

As depicted in Fig. 3 in case of the $H \rightarrow ZZ^{(*)}$ decay for both production processes the signal S and the signal-background interference I for $m_{ZZ} > 2m_Z$ are about an order of magnitude smaller than the background. According to Fig. 4 in case of $H \rightarrow WW^{(*)}$ for both production processes, however, more background diagrams lead to a further suppression of the signal to background ratio S/B . The absolute contribution from the interference term I gains in its relative size with respect to the signal S and easily exceeds it. We quantify the signal to background ratio below in Tab. 3. For $e^+e^- \rightarrow \nu\bar{\nu}VV$ the interference structures in Fig. 3 and Fig. 4 at $m_{VV} = \sqrt{s} - m_Z$ are induced by the process $e^+e^- \rightarrow ZVV$ followed by $Z \rightarrow \nu\bar{\nu}$. The latter process is kinematically strongly suppressed for larger invariant masses, since the Z boson decaying into a pair of (anti-)neutrinos needs to be off-shell for $m_{VV} > \sqrt{s} - m_Z$.

The (s -channel) Higgs induced contributions $e^+e^- \rightarrow ZH \rightarrow ZVV \rightarrow \nu\bar{\nu}VV$, where all neutrino flavours need to be taken into account, are treated as a background to $e^+e^- \rightarrow \nu\bar{\nu}VV$. However, the relevance of Higgs induced contributions including $Z \rightarrow \nu\bar{\nu}$ for the final state $\nu\bar{\nu}VV$ is small. Multiplying Higgsstrahlung $e^+e^- \rightarrow ZH$ with the branching ratio $\text{BR}(Z \rightarrow \nu\bar{\nu}) \approx 20\%$ yields cross sections smaller than the ones through vector boson fusion $e^+e^- \rightarrow \nu\bar{\nu}H$ even for energies $\sqrt{s} < 500$ GeV. Additional cuts can moreover further reduce the amount of Higgsstrahlung in $e^+e^- \rightarrow \nu\bar{\nu}VV$, since the two neutrinos in vector boson fusion only induce a relatively small missing transverse energy/momentum.

We quantify the signal/background ratio by defining

$$\Delta_{\text{SB}}^{ZVV} = \frac{\sigma_{\text{off}}^{ZVV}(130\text{GeV}, \sqrt{s} - m_Z)}{\sigma_{\text{all}}^{ZVV}(130\text{GeV}, \sqrt{s} - m_Z)} \quad \text{and} \quad \Delta_{\text{SB}}^{\nu\bar{\nu}VV} = \frac{\sigma_{\text{off}}^{\nu\bar{\nu}VV}(130\text{GeV}, \sqrt{s})}{\sigma_{\text{all}}^{\nu\bar{\nu}VV}(130\text{GeV}, \sqrt{s})} \quad , \quad (8)$$

where σ_{all} includes S , I and B contributions, whereas σ_{off} just contains the signal contributions $e^+e^- \rightarrow ZH \rightarrow ZVV$ and $e^+e^- \rightarrow \nu\bar{\nu}H \rightarrow \nu\bar{\nu}VV$ as before. The results for different cms energies are presented in Tab. 3. Again we distinguish between the pure usage of Eq. (5), $e^+e^- \rightarrow ZH \rightarrow Z_1Z_2Z_3$, for the signal contribution and the inclusion of all Higgs induced diagrams for the process $e^+e^- \rightarrow ZH \rightarrow ZZZ$, where an averaging over the three ZZ pairs is implied. Again we would like to stress that for the full process $e^+e^- \rightarrow ZZZ$ the averaging over the three ZZ pairs is obsolete. Similarly, for $e^+e^- \rightarrow \nu\bar{\nu}WW$ we add the t -channel Higgs contributions to capture all Higgs induced diagrams.

\sqrt{s}	$\sigma_{\text{all}}^{ZZZ}$	$\Delta_{\text{SB}}^{Z_1Z_2Z_3} (\Delta_{\text{SB}}^{ZZZ})$	$\sigma_{\text{all}}^{\nu\bar{\nu}ZZ}$	$\Delta_{\text{SB}}^{\nu\bar{\nu}ZZ}$
250 GeV	---	---	1.51 fb	0.04 %
300 GeV	0.34 fb	3.19(12.9) %	1.36 fb	0.33 %
350 GeV	1.19 fb	2.62(11.9) %	1.66 fb	1.01 %
500 GeV	2.06 fb	2.83(11.6) %	2.85 fb	4.96 %
1 TeV	1.71 fb	4.40(10.2) %	16.7 fb	11.6 %
\sqrt{s}	$\sigma_{\text{all}}^{ZWW}$	Δ_{SB}^{ZWW}	$\sigma_{\text{all}}^{\nu\bar{\nu}WW}$	$\Delta_{\text{SB}}^{\nu\bar{\nu}WW}$
250 GeV	---	---	0.05 fb	9.87(9.87) %
300 GeV	7.34 fb	3.27 %	1.68 fb	1.57(1.42) %
350 GeV	29.2 fb	1.30 %	6.44 fb	1.18(1.03) %
500 GeV	91.8 fb	0.53 %	22.4 fb	2.05(1.63) %
1 TeV	136.7 fb	0.37 %	67.3 fb	7.31(4.49) %

Table 3: Inclusive cross sections $\sigma_{\text{all}}(130\text{GeV}, \sqrt{s} - m_Z)$ for $e^+e^- \rightarrow ZH \rightarrow ZVV$ and $\sigma_{\text{all}}(130\text{GeV}, \sqrt{s})$ for $e^+e^- \rightarrow \nu\bar{\nu}H \rightarrow \nu\bar{\nu}VV$ for $\text{Pol}(e^+, e^-) = (0.3, -0.8)$ and for different cms energies \sqrt{s} and relative size of the signal/background ratio Δ_{SB} in %. In brackets we add the results averaging over the three ZZ pairs for $e^+e^- \rightarrow ZZZ$ and taking into account the t -channel Higgs contribution for $e^+e^- \rightarrow \nu\bar{\nu}WW$.

As it can be seen from Tab. 3 Δ_{SB} is rather constant for $e^+e^- \rightarrow ZZZ$ and increases with energy for $e^+e^- \rightarrow \nu\bar{\nu}VV$, if the very small cross section for $e^+e^- \rightarrow \nu\bar{\nu}WW$ for the cms energy $\sqrt{s} = 250$ GeV is not taken into account. For $e^+e^- \rightarrow ZWW$ instead the ratio Δ_{SB} decreases with the cms energy. In all cases Δ_{SB} is of order 1 – 10 % in the relevant regions of the production processes. The influence of the signal-background interference is possibly even larger and thus the prospects concerning the sensitivity to the Higgs contributions look

promising. In contrast to Δ_{off} the signal/background ratio Δ_{SB} is dependent on the initial polarisation, as it can also be seen from Fig. 7. In Section 5 we will perform a simulation with fermionic/hadronic final states for $e^+e^- \rightarrow \nu\bar{\nu} + 4\text{jets}$ to investigate the significance in terms of event rates. However, we can only provide rough estimates and a rather qualitative discussion. Further studies taking into account higher order corrections, beamstrahlung, hadronization of jets and a proper detector simulation would be desirable.

4 Phenomenological implications of off-shell contributions

In this section we want to investigate the consequences of the off-shell Higgs contributions for the Z recoil method and the extraction of HVV couplings. Moreover, we comment on their role for unitarity cancellations in gauge boson scattering and their possible impact on constraining higher-dimensional operators, which can, for instance, be induced in composite Higgs scenarios. The connection to the Higgs width is analysed in the subsequent sections.

4.1 Z recoil method

As pointed out, the Z recoil mass measurement is a key feature of a linear collider which allows to access the production process $e^+e^- \rightarrow ZH$ through the decays of the Z boson only, so that an absolute measurement of the production cross section is possible. The analysis is primarily based on the decays $Z \rightarrow e^+e^-/\mu^+\mu^-$ [37], where by the invariant mass and the energy of the l^+l^- system the reconstructed mass \hat{m}_Z and the energy E_Z of the Z boson are obtained. Recently also hadronic final states were discussed [51, 52]. The recoil mass m_R is computed according to

$$m_R^2 = s + \hat{m}_Z^2 - 2E_Z\sqrt{s} \quad (9)$$

and thus equals the invariant mass of the Higgs boson p_H^2 . According to our discussion off-shell effects in Higgs boson decays manifest themselves in the differential cross section $d\sigma/dm_R$, which we demonstrate in Fig. 8 for the Higgsstrahlung production process. The figures show the results obtained by Eq. (5), where the invariant mass m_{VV} is replaced by m_R , combined with the sum over the partial decays $H \rightarrow ZZ^{(*)}, WW^{(*)}, b\bar{b}, t\bar{t}, gg, \tau^+\tau^-$ as provided by the LHC-HXSWG. The increase in the differential cross section at the thresholds $m_R = 2m_W$ and $m_R = 2m_Z$ is clearly visible. Moreover at $m_R = 2m_t$ additionally the decay $H \rightarrow t\bar{t}$ opens kinematically. In order to quantify the off-shell contributions we use again Δ_{off} defined in Eq. (7) translated to $e^+e^- \rightarrow ZH \rightarrow Z + X$ with m_R instead of m_{VV} and present the results in Tab. 4.

\sqrt{s}	250 GeV	300 GeV	350 GeV	500 GeV	1 TeV
Δ_{off}	0.02 %	0.12 %	0.30 %	0.91 %	1.84 %

Table 4: Off-shell contributions for the signal cross section determined via the Z recoil method.

As expected from the analysis of Fig. 3 and Fig. 4, the off-shell contributions are unimportant for the case of $\sqrt{s} = 250$ GeV. Because of the presence of the decay mode $H \rightarrow b\bar{b}$, which dominates for $m_R = 120 - 130$ GeV, and of the other relevant decay modes for a SM-like Higgs, the off-shell effects induced by the $H \rightarrow ZZ^{(*)}$ and $H \rightarrow WW^{(*)}$ modes are

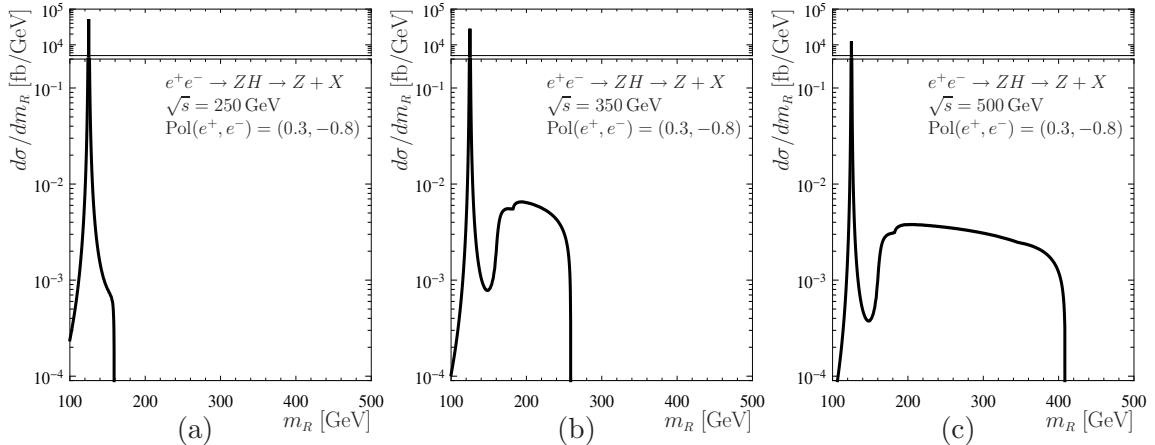


Figure 8: $d\sigma/dm_R$ in fb/GeV as a function of m_R in GeV for $e^+e^- \rightarrow ZH \rightarrow Z + X$ defined in Eq.(5) (with m_{VV} replaced by m_R) combined with the sum over $H \rightarrow X = ZZ^{(*)}, WW^{(*)}, b\bar{b}, t\bar{t}, gg, \tau^+\tau^-$ for a fixed polarisation $\text{Pol}(e^+, e^-) = (0.3, -0.8)$ and cms energies (a-c) $\sqrt{s} = 250, 350, 500$ GeV.

less pronounced than in Fig. 3 and Fig. 4, but still clearly visible in Fig. 8 for $\sqrt{s} = 350$ GeV and $\sqrt{s} = 500$ GeV. For $\sqrt{s} = 500$ GeV the off-shell contributions amount to about 1% (at $\sqrt{s} = 1$ TeV they are close to 2%). While these off-shell effects are relatively small, for $\sqrt{s} = 500$ GeV and above they are nevertheless relevant for analyses aiming at an accuracy at the percent level. The potential problem caused by the presence of off-shell contributions is that the cross section that is determined via the recoil method actually contains a non-negligible amount of off-shell contributions, while it is interpreted as an on-shell cross section. The impact of the off-shell contributions can be reduced by appropriate cuts, for instance a cut on the recoil mass $m_R \in [115, 150]$ GeV. Some care is necessary in this case in order to determine the appropriate efficiencies. In case of $H \rightarrow ZZ^{(*)}$, where another on-shell Z boson is involved in the process, a misidentification of the Z boson out of the Higgsstrahlung process can occur. Again in the most pessimistic approach an average over the final state Z bosons is performed, which we included in Fig. 8. We note that this averaging and thus the misidentification of ZZ pairs lowers the total on-shell cross section by about 1 – 2% compared to the correct discrimination of all ZZ pairs.

While the effects of the off-shell contributions on the determination of the production cross section via the Z recoil method have turned out to be relatively small, our analysis nevertheless adds to the motivation for performing the cross-section determination via the Z recoil method close to threshold, i.e. at about $\sqrt{s} = 250 - 350$ GeV, rather than at higher energies where the off-shell effects become relevant.

4.2 HVV couplings, unitarity and higher-dimensional operators

Off-shell contributions also play a role for the extraction of HVV couplings at an e^+e^- collider. While in the studies carried out so far usually the validity of the ZWA has been assumed, for precision analyses it will be important to discriminate the on-shell coupling g_{HVV}^{on} from off-shell contributions, $g_{HVV}(m_{VV})$, through appropriate cuts on the invariant mass of the decay products. An analysis where this will be relevant is for example the determination

of the HWW coupling from $e^+e^- \rightarrow \nu\bar{\nu}H \rightarrow \nu\bar{\nu}WW$ at $\sqrt{s} = 500$ GeV [39, 53], where both on- and off-shell Higgs contributions are present. As mentioned in Section 3.1, for accurate predictions of processes involving the decay of an on-shell Higgs boson into weak bosons and thus for the determination of g_{HVV}^{on} also a precise knowledge of the Higgs mass m_H will be crucial.

Off-shell Higgs induced contributions in the scattering of longitudinal gauge bosons are known to be of crucial importance for preserving unitarity. The corresponding amplitude involving contributions from the gauge sector increases with the square of the cms energy in the high-energy limit. This bad high-energy behaviour is cancelled by Higgs-exchange contributions in models where a Higgs sector with at least one fundamental scalar particle gives rise to electroweak symmetry breaking. Accordingly, the interference term between the Higgs-exchange and the background contributions is large and negative, as discussed in Section 3.2. Detailed studies of high-energy vector boson scattering are an essential test for electroweak symmetry breaking. The investigation of deviations from the SM prediction in form of effective field theories requires the application of a unitarization prescription [54].

The off-shell Higgs contributions are known to be a sensitive probe in particular of compositeness [55] described through higher-dimensional operators [56], which affect $WW \rightarrow WW/HH$. A detailed study on the sensitivity of $e^+e^- \rightarrow \nu\bar{\nu}VV$ with subsequent $VV \rightarrow 4$ jets can be found in Ref. [57]. We will also discuss the Higgs induced contributions to this process and the process $e^+e^- \rightarrow \mu^+\mu^- + 4$ jets in the following. For the case of the LHC and collider-independent statements we refer to the studies presented in Refs. [30–34, 58].

5 Processes $e^+e^- \rightarrow \nu\bar{\nu} + 4$ jets and $e^+e^- \rightarrow \mu^+\mu^- + 4$ jets

In order to work out the practical consequences of our discussion and to investigate the sensitivity to off-shell Higgs contributions, we have performed a Monte Carlo simulation of the partonic process $e^+e^- \rightarrow \nu\bar{\nu} + 4$ jets using `MadGraph5_aMC@NLO` at leading order. We present results for an integrated luminosity of $\int \mathcal{L} dt = 500 \text{ fb}^{-1}$ at energies $\sqrt{s} = 350, 500$ GeV and 1 TeV for a polarisation of the initial state of $\text{Pol}(e^+, e^-) = (0.3, -0.8)$. In Section 6 we shortly discuss the changes due to the inclusion of initial state radiation, which also allows one to estimate effects of beamstrahlung. Moreover the inclusion of higher-order contributions is described within this section.

The first process that we consider is $e^+e^- \rightarrow \nu\bar{\nu} + 4$ jets. This process is suitable for the investigation of off-shell contributions for several reasons: the $H \rightarrow ZZ^{(*)}$ and $H \rightarrow WW^{(*)}$ decays both give rise to 4 jet final states with a relatively high event rate, and the invariant mass of the intermediate Higgs can be reconstructed from the decay products (without the need for averaging between different final states). For the theoretical prediction we include all three neutrino flavours in the final state (i.e., not only the electron neutrinos produced in the diagram of Fig. 1b). A jet is understood as being either a gluon or one of the (anti-)quarks u, d, s, c . In contrast a b -(anti-)quark in the final state would change the picture due to the decay $H \rightarrow b\bar{b}$. It should be noted that we do not employ parton showering/hadronization, but denote (anti-)quarks and gluons as final state jets. For a jet we demand a minimum transverse momentum of $p_T > 20$ GeV, a maximal rapidity of $|y| < 5$ and $\Delta_R \equiv \sqrt{(\Delta\phi)^2 + (\Delta y)^2} > 0.4$ between the various jets to allow for jet separation. $\Delta\phi$ and Δy denote the azimuthal angular and rapidity differences between two jets. For a massless particle the rapidity $y = 5$

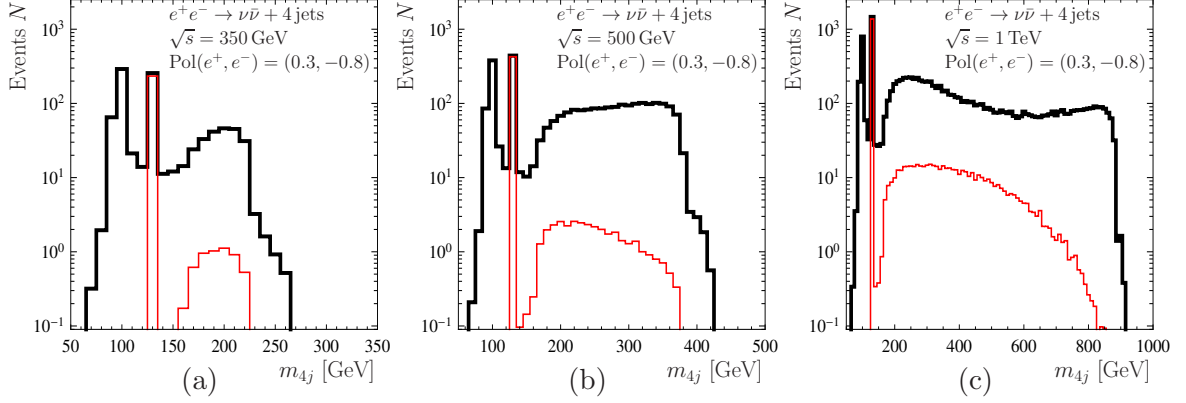


Figure 9: Event rates for $e^+e^- \rightarrow \nu\bar{\nu} + 4\text{jets}$ for $\int \mathcal{L} dt = 500 \text{ fb}^{-1}$ as a function of the invariant mass of the 4 jets m_{4j} in bins of 10 GeV width after the cut $p_{T,4j} > 75 \text{ GeV}$ for (a) $\sqrt{s} = 350 \text{ GeV}$, (b) $\sqrt{s} = 500 \text{ GeV}$ and (c) $\sqrt{s} = 1 \text{ TeV}$. The Higgs-induced contributions are shown in red.

corresponds to an opening angle of 0.77° between the particle three-momentum and the beam axis. As explained below the transverse momentum of all four jets $p_{T,4j}$ is required to be larger than 75 GeV to reduce background from the process $e^+e^- + 4\text{jets}$.

We show our results in Fig. 9. The red contribution includes only (s -channel) Higgs induced contributions, as discussed in previous sections, and corresponds to an estimate of signal and interference contributions. In those we exclude contributions where the 4 jets do not stem from a Higgs. The latter case can occur in case of $e^+e^- \rightarrow ZH$ followed by $Z \rightarrow jj$ and $H \rightarrow \nu\bar{\nu}jj$. The treatment of interference terms between $e^+e^- \rightarrow ZH, Z \rightarrow jj, H \rightarrow \nu\bar{\nu}jj$ and the signal contributions is not straightforward, and we count those interference contributions as part of the signal (red). However, since the Higgsstrahlung production process $e^+e^- \rightarrow ZH$ multiplied with an additional branching ratio is essentially irrelevant for $\sqrt{s} > 500 \text{ GeV}$, the net effect of this kind of contributions is negligible. Also for $\sqrt{s} = 350 \text{ GeV}$ the effect is rather small. We note that the indicated signal contribution is — of course — not a physical observable. Our aim here is to merely illustrate the relevance of Higgs-induced contributions (assuming SM-like couplings) in comparison with the full cross section, i.e. the total number of events. Even more important than the signal S indicated in red is the signal-background interference I , which for the process under consideration is negative. Within the SM at high cms energies, where VBF dominates, its absolute size is larger than S , such that the inclusion of the Higgs-induced contributions lowers the total number of events.

We quantify the number of Higgs-induced events, indicated as signal in Fig. 9, as N_H in Tab. 5 and add the number of events without Higgs contribution in any Feynman diagram N_{woH} , which allows to read off the impact of the interference term I when comparing to the total number of events N . In particular at $\sqrt{s} = 1 \text{ TeV}$ the off-shell contributions give rise to a sizable fraction of the total number of events. At low energies, on the other hand, the sensitivity to off-shell contributions is statistically limited. The relevance of Higgs off-shell events in $e^+e^- \rightarrow \nu\bar{\nu} + 4\text{jets}$ can be enhanced by enforcing VBF induced final states by e.g. setting an upper limit on the missing transverse energy (MET) in energy regions where VBF dominates over Higgsstrahlung.

A potentially large background to $e^+e^- \rightarrow \nu\bar{\nu} + 4\text{jets}$ is induced by the final state $e^+e^- +$

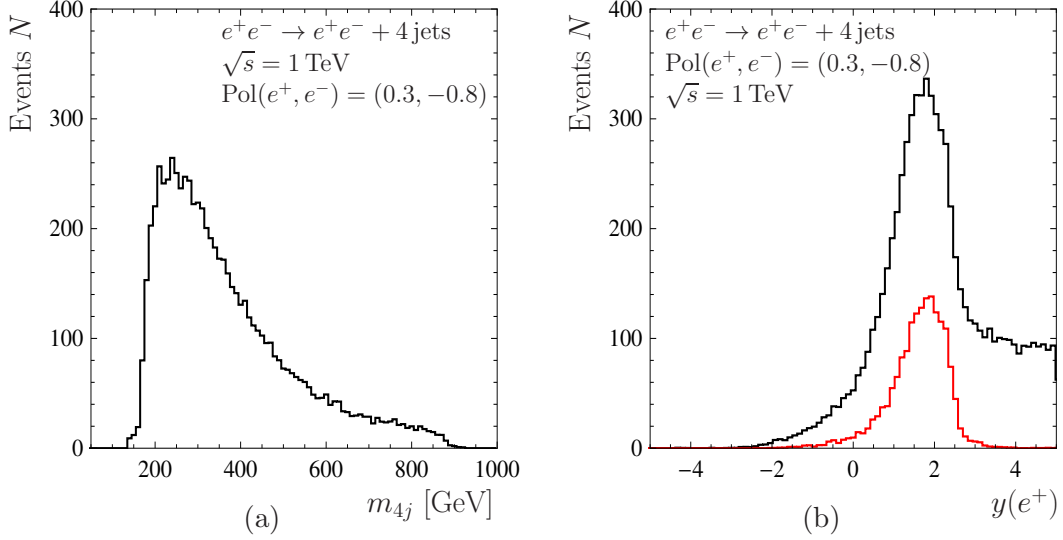


Figure 10: Event rates for $e^+e^- \rightarrow e^+e^- + 4 \text{ jets}$ for $\sqrt{s} = 1 \text{ TeV}$ and $\int \mathcal{L} dt = 500 \text{ fb}^{-1}$ after the cuts $m_{4j} > 130 \text{ GeV}$ and $p_{T,4j} > 75 \text{ GeV}$ as a function of (a) the invariant mass of the 4 jets m_{4j} ; (b) the rapidity of the positron $y(e^+)$. In the right plot we show in red events with $|y(e^+)| > 2.5$, out of which events with $|y(e^+)| > 2.5$ correspond to the background N_B (see text).

4 jets, where the two leptons remain undetected, i.e. stay close to the beam pipe. We assume here that leptons can be reconstructed up to rapidities of $|y| < 2.5$, which for a massless particle corresponds to an angle of 9.38° between particle three-momentum and beam axis. Thus, the background can be strongly suppressed by a lower cut on the transverse momentum of the four jets $p_{T,4j} > 75 \text{ GeV}$, which forces the electron and positron to have a combined p_T of more than 75 GeV and thus rather small rapidities. Accordingly, this cut was introduced already in our investigation of the process $e^+e^- \rightarrow \nu\bar{\nu} + 4 \text{ jets}$ (see the results shown in Fig. 9 above), where less events are lost by the requirement $p_{T,4j} > 75 \text{ GeV}$, even for VBF. The remaining number of background events from the process $e^+e^- + 4 \text{ jets}$ is denoted by N_B in Tab. 5. In Fig. 10 we show distributions for the process $e^+e^- \rightarrow e^+e^- + 4 \text{ jets}$ applying the cuts $m_{4j} > 130 \text{ GeV}$ and $p_{T,4j} > 75 \text{ GeV}$, but at first allowing for arbitrary rapidities of both leptons. The relevant background events N_B are those with rapidities $|y(e^\pm)| > 2.5$, which can be deduced from Fig. 10 (b).

It should be noted that the process $e^+e^- \rightarrow e^+e^- + 4 \text{ jets}$ of course includes Higgs-induced events. However, the cross section of Z boson fusion is considerably smaller than the one of W boson fusion, and for Higgsstrahlung including $Z \rightarrow e^+e^-$ the probability that both leptons escape undetected is small. In that manner $e^+e^- \rightarrow e^+e^- + 4 \text{ jets}$ with undetected leptons can be considered as a pure background contribution.

As a second example we consider the process $e^+e^- \rightarrow \mu^+\mu^- + 4 \text{ jets}$, where we again demand a minimum transverse momentum of $p_T > 20 \text{ GeV}$ for the jets, a maximal rapidity of $|y| < 5$ and $\Delta_R > 0.4$ between the various jets to ensure jet separation. Concerning the detection of the two final state leptons, we again assume that a rapidity of $|y| < 2.5$ is required. In contrast to the previous process, the final state $\mu^+\mu^- + 4 \text{ jets}$ is not induced by VBF and therefore shows a generally smaller interference term, but necessarily also overall

\sqrt{s}	350 GeV	500 GeV	1 TeV
N	265	1793	7994
N_H	6	34	510
N_{woH}	256	1771	8298
N_B	0	0	65

Table 5: Number of events N with $m_{4j} > 130$ GeV and $p_{T,4j} > 75$ GeV for $e^+e^- \rightarrow \nu\bar{\nu} + 4\text{jets}$ for $\int \mathcal{L} dt = 500 \text{ fb}^{-1}$. N_H corresponds to the (s -channel) Higgs induced events. N_{woH} is the number of events without any Higgs contribution allowing to estimate the interference I . N_B are background events due to $e^+e^- \rightarrow e^+e^- + 4\text{jets}$ (see text).

smaller event rates. The sensitivity of both processes to effects of the Higgs-boson width will be investigated in Section 7.

6 Initial state radiation and higher-order effects

In this section we want to investigate the impact of the inclusion of initial state radiation and other higher-order effects. For this purpose we have repeated our study for the process $e^+e^- \rightarrow \nu_e\bar{\nu}_e u\bar{d}s\bar{c}$, being a subprocess of $e^+e^- \rightarrow \nu\bar{\nu} + 4\text{jets}$, with the code `LUSIFER` [59], which allows the user to apply different schemes for the treatment of finite widths and to include initial state radiation. We choose $\sqrt{s} = 500$ GeV, $\text{Pol}(e^+, e^-) = (0.3, -0.8)$ and require for a minimum jet energy of 10 GeV. Since $p_{T,4j}$ is only nontrivially accessible in `LUSIFER` the corresponding cut is not applied, however for each outgoing (anti-)quark a minimal energy of $E_q > 10$ GeV is required. The inclusive cross sections obtained with `LUSIFER` and `MadGraph5_aMC@NLO` agree at lowest order without the inclusion of initial state radiation within their numerical errors applying the cut of $E_q > 10$ GeV for each outgoing (anti-)quark. We have also verified that the predictions of the two codes for the differential cross section as function of the invariant mass of the four quarks agree with each other very well. We choose input-parameter scheme 2 of `LUSIFER` and include gluonic contributions, which are however tiny and also part of the `MadGraph5_aMC@NLO` result. In order to test the reliability of the prediction in the high invariant mass region, we choose different width schemes for the gauge bosons and find negligible differences. In particular the usage of a fixed width leads to results that just differ at the permil level from the ones obtained using a complex-pole scheme, even for large invariant masses of the four quarks final state. The effect of initial state radiation turns out to be more relevant. It reduces the overall cross section by a few percent and affects mostly the region of high invariant masses, see Fig. 11.

A similar effect can be expected from the inclusion of beamstrahlung. Thus, both effects should be taken into account for precision analyses, but they do not change the qualitative features of our results. The inclusion of higher-order corrections is expected to have a bigger impact for $e^+e^- \rightarrow \nu_e\bar{\nu}_e W^+W^-$, as reported in Ref. [60]. In Ref. [60] the corrections have been calculated in the equivalent vector-boson approximation. This approximation only includes diagrams involving the subprocess $WW \rightarrow WW$, and the quality of this approximation is expected to improve with increasing cms energy. However, even in the high mass region this approximation has been found to depart by up to 10% from the exact matrix element calculation at tree-level. Nevertheless, this method can serve as an estimate of the impact of

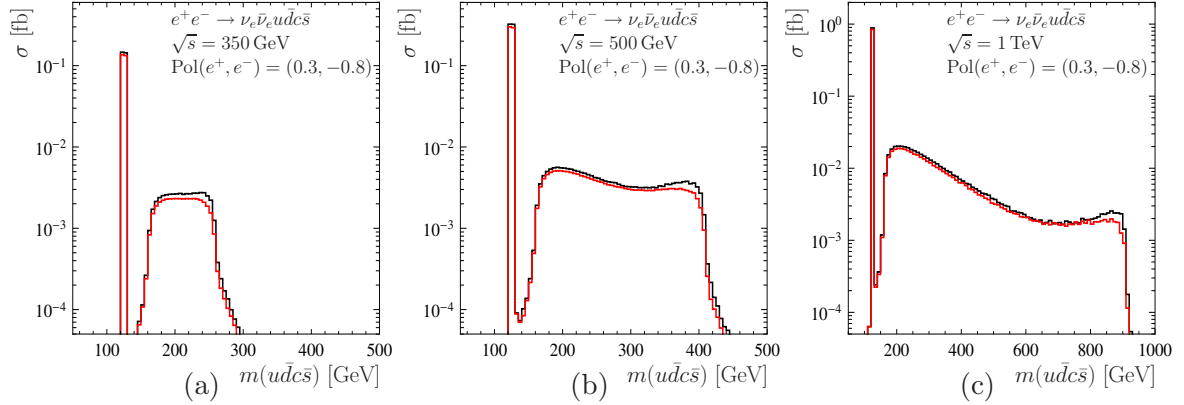


Figure 11: Cross section for $e^+e^- \rightarrow \nu_e \bar{\nu}_e u \bar{d} c \bar{s}$ in fb in bins as a function of $m(u \bar{d} c \bar{s})$ in GeV for (a) $\sqrt{s} = 350$ GeV, (b) $\sqrt{s} = 500$ GeV and (c) $\sqrt{s} = 1$ TeV. The black curves show the results without and the red curves the results including initial state radiation.

higher-order effects: the (logarithmic) electroweak higher-order corrections for $\sqrt{s} = 1$ TeV reach -6.7% , where several cuts like e.g. $m_{WW} > 400$ GeV have been employed. However, the correction strongly increases with the invariant mass of the gauge bosons and amounts up to -20% in the region $m_{VV} = 700 - 800$ GeV. Thus, higher-order effects are relevant in this context and should be taken into account for a precise analysis of off-shell effects. As one can see from the dependence of the corrections on the invariant mass, this kind of corrections can in general not be taken into account by a simple global “K-factor”.

7 Constraints on the Higgs width

For the reconstruction of the width of the Higgs boson, Γ_H , the linear collider offers a unique method through the measurement of the recoil against the Z boson in $e^+e^- \rightarrow ZH$ in combination with the measurement of branching ratios. The method was already discussed in Section 4.1. It is based on the validity of the ZWA

$$\sigma_{\text{ZWA}} = \frac{\sigma_{A \rightarrow H} \Gamma_{H \rightarrow B}}{\Gamma_H} \propto \frac{(g_A^{\text{on}} g_B^{\text{on}})^2}{\Gamma_H}, \quad (10)$$

where the index “on” refers to on-shell couplings. Running an e^+e^- collider at rather low cms energies of $\sqrt{s} = 250 - 350$ GeV, the Z recoil method allows to determine $\sigma_{e^+e^- \rightarrow ZH}$ and thus $(g_{HZZ}^{\text{on}})^2$ by just observing the decay products of the Z boson into leptons. Recently also Z boson decays into hadrons were discussed, which provide a higher sensitivity, but on the other hand are more difficult to distinguish from Higgs decays [51, 52]. By a combination of various final states of the Higgs decays (see e.g. Ref. [38]) the Higgs width Γ_H can be extracted, in case the ZWA is valid or at least off-shell contributions can be reduced by reasonable cuts.

7.1 Combination of on- and off-shell contributions

On the other hand, similar to proposed methods at the LHC [12–14, 19–22], the combination of on- and off-shell contributions can be used to obtain constraints on the Higgs width. We will discuss this method and the underlying assumptions in the following.

Changing the product of the squared couplings entering the production cross section and the partial decay width by a common factor leaves the inclusive on-shell cross section σ_{ZWA} in Eq. (10) unchanged, if at the same time the total width appearing in the denominator of Eq. (10) is rescaled accordingly. For instance, for the process $e^+e^- \rightarrow ZH \rightarrow ZZZ$ the inclusive on-shell cross section can be expressed by scale factors relative to the SM cross section [11, 61],

$$\sigma_{\text{ZWA}}^{\text{ZZZ}} = \frac{(\kappa_Z^{\text{on}})^4}{r} \sigma_{\text{ZWA}}^{\text{ZZZ,SM}} =: \mu_{\text{on}}^{\text{ZZZ}} \sigma_{\text{ZWA}}^{\text{ZZZ,SM}} \quad , \quad (11)$$

where $\kappa_V^{\text{on}} = g_{HVV}^{\text{on}}/g_{HVV}^{\text{on,SM}}$, $r = \Gamma_H/\Gamma_H^{\text{SM}}$, and μ_{on} is the signal strength obtained from on-shell measurements for the process under consideration. Similarly, for the Higgs induced processes $e^+e^- \rightarrow ZWW/\nu\bar{\nu}ZZ/\nu\bar{\nu}WW$ the scale factors in the numerator read $\kappa_Z^2\kappa_W^2$, $\kappa_Z^2\kappa_W^2$ and κ_W^4 , respectively. The off-shell contributions are not proportional to $1/\Gamma_H$, but depend on the off-shell propagator, see e.g. Eq. (5). In the approximation where the dependence of the off-shell propagator on the total width is neglected, the off-shell cross section can formally be expressed in terms of off-shell scale factors² as

$$\frac{d\sigma_{\text{off}}^{\text{ZZZ}}}{dm_{ZZ}} = (\kappa_Z^{\text{off}}(m_{ZZ}))^4 \frac{d\sigma_{\text{off}}^{\text{ZZZ,SM}}}{dm_{ZZ}} = \mu_{\text{off}}^{\text{ZZZ}}(m_{ZZ}) \frac{d\sigma_{\text{off}}^{\text{ZZZ,SM}}}{dm_{ZZ}} \quad \text{for} \quad m_{ZZ} > m_H \quad . \quad (12)$$

The off-shell scale factors $\kappa^{\text{off}}(m_{VV})$ and signal strengths $\mu_{\text{off}}(m_{VV})$ depend in general on the invariant mass m_{VV} . The change in the scale factors for different values of m_{VV} arises from the running of the couplings induced by loop contributions and in particular from threshold effects associated with additional particles beyond the SM. If effects of this kind are disregarded and it is assumed that the off-shell scale factors $\kappa^{\text{off}}(m_{VV})$ can be set equal to their on-shell values κ^{on} for the whole considered range of m_{VV} values, the ratio of the off-shell and on-shell signal strengths provides information about the total width,

$$\frac{\mu_{\text{off}}(m_{VV})}{\mu_{\text{on}}} = r \quad \text{for} \quad \kappa^{\text{off}}(m_{VV}) = \kappa^{\text{on}} \quad . \quad (13)$$

In particular, an upper bound on the total width can be obtained under those assumptions from the measurement of μ_{on} and the determination of an upper bound on $\mu_{\text{off}}(m_{VV})$. This procedure can be repeated for all final states independently.

The question how well the off-shell contribution of the signal can be discriminated against the background clearly plays an important role regarding the sensitivity that can be achieved with this method. In this context the signal-background interference I for $m_{VV} > 2m_V$ is of large relevance, see Section 3.2. Assuming that the background behaves SM-like, the interference term I is expected to scale like $\sqrt{\mu_{\text{off}}(m_{VV})} = \sqrt{\mu_{\text{on}}r}$. The interference term yields a mostly negative contribution and thus lowers the sensitivity to the Higgs width. In our numerical analysis below we assume that the measured value for the on-shell cross section agrees with the SM value, i.e. $\mu_{\text{on}} = 1$, and we furthermore assume $\kappa_V \equiv \kappa_Z = \kappa_W$ for simplicity.

²The extension of the concept of tree-level inspired scale factors κ_i to off-shell quantities is in general questionable, see the discussion in Ref. [62]. We merely use off-shell scale factors in a formal sense here as a shorthand for the parametrisation of deviations from the SM.

7.2 Impact of BSM contributions

The method described above relies on the strong theoretical assumption that the effective couplings far off-shell are the same as their on-shell counterparts. The relation between $\kappa^{\text{off}}(m_{VV})$ and κ^{on} can however be severely affected by contributions from physics beyond the SM (BSM), in particular via threshold effects. In fact, BSM effects of this kind may actually be needed to give rise to a Higgs-boson width that differs from the one of the SM by the amount that is currently probed in the analyses at the LHC. Examples for the possible impact of BSM effects on the LHC analyses have recently been investigated in Refs. [31, 63–65]. In particular, in Ref. [64] the validity of the Higgs width bound has been discussed in different BSM models, and non-resonant and resonant contributions in the off-shell region have been classified. As an example, squark contributions in the minimal supersymmetric standard model (MSSM) or its simplest extension by adding a singlet (NMSSM) can alter the off-shell region by non-resonant contributions affecting the gluon fusion production cross section at the LHC. It should be noted that even the pure SM loop contribution from top quarks to the decay of an off-shell Higgs boson, $H \rightarrow VV$, show a sensitive dependence on m_{VV} , in particular across the threshold where $m_{VV} = 2m_t$. The description of those loop contributions in terms of a universal, i.e. m_{VV} -independent, scale factor is therefore a rather poor approximation in the off-shell region.

In contrast to the loop-induced gluon fusion production process at the LHC, the corresponding processes at an e^+e^- collider are a priori less affected by loop contributions of BSM particles, since those loop contributions have to compete with the leading tree-level type contributions to Higgs production at an e^+e^- collider. Nevertheless, sizeable effects in the off-shell contributions could also arise from the presence of additional Higgs bosons at tree level, see e.g. Ref. [65].

7.3 Application to the linear collider and LHC implications

In the following we want to investigate which sensitivity one obtains at a linear collider for constraining the Higgs width from the comparison of on-shell and off-shell contributions, if one uses the same assumption about the equality of the on-shell and off-shell effective couplings as in the LHC analyses. Because of the discussed problems of this assumption regarding the possible presence of sizeable BSM contributions, we focus our attention to the region where the Higgs width differs from the SM case only by a rather small amount. We consider again the process $e^+e^- \rightarrow \nu\bar{\nu} + 4\text{jets}$ simulated with `MadGraph5_aMC@NL0`. We apply the same cuts as described in Section 5. Assuming an on-shell signal strength of $\mu_{\text{on}} = 1$, the dependence of the number of events on r can be written in the form

$$N(r) = N_0(1 + R_1\sqrt{r} + R_2r) + N_B \quad . \quad (14)$$

N_0 differs from N_{woH} by on-shell Higgs events. N_B are background events $e^+e^- \rightarrow e^+e^- + 4\text{jets}$ with undetected leptons and can be taken from Tab. 5. Their dependence on r is negligible for $r < 10$.

We have performed a simulation for three values of \sqrt{s} corresponding to an integrated luminosity of $\int \mathcal{L} dt = 500 \text{ fb}^{-1}$ at each cms energy. The results for the parameters N_0 , R_1 and R_2 , which we have obtained from a fit, are given in Tab. 6. As expected the interference term, reflected in R_1 , is large and negative and thus lowers the sensitivity around $r \sim 1$.

\sqrt{s}	350 GeV	500 GeV	1 TeV
N_0 ($\int \mathcal{L} dt = 500 \text{ fb}^{-1}$)	263	1775	8420
R_1	-0.017	-0.010	-0.098
R_2	0.026	0.019	0.048
Limit on r ($\int \mathcal{L} dt = 500 \text{ fb}^{-1}$)	7.0	3.8	2.8
Limit on r ($\int \mathcal{L} dt = 1 \text{ ab}^{-1}$)	5.1	3.1	2.5

Table 6: N_0 , R_1 and R_2 as a function of the cms energy for $e^+e^- \rightarrow \nu\bar{\nu} + 4\text{jets}$ with $m_{4j} > 130 \text{ GeV}$ and $p_{T,4j} > 75 \text{ GeV}$. The upper limits on r at 95% have been obtained according to our simplistic Bayesian approach, using the assumptions specified in the text.

The interference term is largest for the largest cms energy, since there the VBF channel dominates. For $\sqrt{s} = 350 \text{ GeV}$ and 500 GeV , on the other hand, the relative importance of the Higgsstrahlung process is higher, reducing the impact of the interference term.

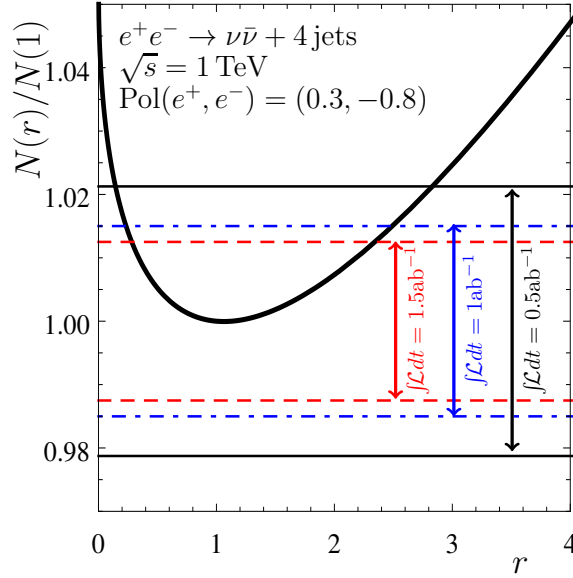


Figure 12: Normalised event rates $N(r)/N(1)$ as a function of r for the process $e^+e^- \rightarrow \nu\bar{\nu} + 4\text{jets}$ for $\sqrt{s} = 1 \text{ TeV}$ and a fixed polarisation with 95% uncertainty bands for different integrated luminosities.

In order to investigate the sensitivity to set bounds on r with this method, we perform a simplistic Bayesian approach: the probability $P(N(r)|N_{\text{obs}})$ with $N(r)$ being the expected number of events and N_{obs} the observed number of events is related to $\mathcal{P}(N_{\text{obs}}|N(r))$ through a prior $\pi(N(r))$, which we assume to be constant in the region of r in the vicinity of $r = 1$ which we are considering here. We furthermore assume that the events are distributed according to a Poisson distribution

$$\mathcal{P}(N_{\text{obs}}|N(r)) = \frac{e^{-N(r)}(N(r))^{N_{\text{obs}}}}{N_{\text{obs}}!} \quad (15)$$

and that the observed rate equals the SM rate, i.e. $N_{\text{obs}} = N(1)$. Accordingly, values of r are excluded in this way if $N_{\text{obs}}(r)$ lies outside of the 95% band of the Poisson distribution

$\mathcal{P}(N_{\text{obs}}|N(r))$. The corresponding exclusion limits for r are also shown in Tab. 6. The interference term I lowers the sensitivity to r even for quite high statistics as it can be seen from Fig. 12, where the exclusion limits on r are shown for three values of the integrated luminosity at $\sqrt{s} = 1$ TeV. The minimum of $N(r)$ is in the vicinity of $r = 1$, so that a measurement of $N(r)$ in this region has the least sensitivity to r . If $N(r)$ differs sufficiently from the minimum value, a high-precision measurement of $N(r)$ could result in a two-fold ambiguity in r . The latter might only be resolved within this method by taking into account different final states.

\sqrt{s}	350 GeV	500 GeV
N_0 ($\int \mathcal{L} dt = 1 \text{ ab}^{-1}$)	430	1024
R_1	0.026	0.006
R_2	0.005	0.006
Limit on r ($\int \mathcal{L} dt = 1 \text{ ab}^{-1}$)	9.5	15
Limit on r ($\int \mathcal{L} dt = 1.5 \text{ ab}^{-1}$)	5.4	8.2

Table 7: N_0 , R_1 and R_2 as a function of the cms energy for $e^+e^- \rightarrow \mu^+\mu^- + 4\text{jets}$ with $m_{4j} > 130$ GeV. The upper limits on r at 95% have been obtained according to our simplistic Bayesian approach, using the assumptions specified in the text.

For the process $e^+e^- \rightarrow \mu^+\mu^- + 4\text{jets}$ the situation is different, since for this process the interference term is positive and also no background events of the type N_B as specified in Eq. (14) need to be considered. The corresponding results are shown in Tab. 7. However, for this process the achievable statistics limits the sensitivity to the Higgs width via this method.

In total we conclude from this investigation that the comparison of on-shell and off-shell contributions at a linear collider provides constraints on the Higgs width that are complementary to the ones that can be obtained from the Z recoil method yielding absolute branching-ratio measurements in combination with the determination of a partial width. The numbers obtained from our simplistic approach can certainly be improved by a better suited analysis identifying intermediate states, choosing different polarisations of the initial state and applying more sophisticated cuts. It can however be inferred that this method, besides relying heavily on theoretical assumptions, requires very high statistics and is limited by the negative interference term. Thus, we find that the approach based on the absolute branching-ratio measurements from the Z recoil remains the by far superior method for determining the Higgs width at a linear collider, both because of its model-independence and the much higher achievable precision.

The qualitative features of our analysis for a linear collider can also be applied to the case of the LHC. In Fig. 13 we show the normalised event rates $N(r)/N(1)$ from the CMS analysis presented in Ref. [28] for the four lepton final state ($4l$) as well as for the two lepton and two neutrino final state ($2l2\nu$) in dependence of the production mechanism after applying suitable cuts. Since background events have been omitted in those plots, no scale is indicated for $N(r)/N(1)$. The $4l$ final state just includes $H \rightarrow ZZ^{(*)}$ contributions, whereas the $2l2\nu$ final state also contains $H \rightarrow WW^{(*)}$ contributions. All curves show a behaviour that is very similar to what we found in our analysis for a linear collider. With increasing statistics the sensitivity to r in the vicinity of $r = 1$ is also considerably reduced at the LHC due to the negative interference term. Similar conclusions are obtained from the ATLAS result [29] as well as from the various theoretical works [19–21, 24].

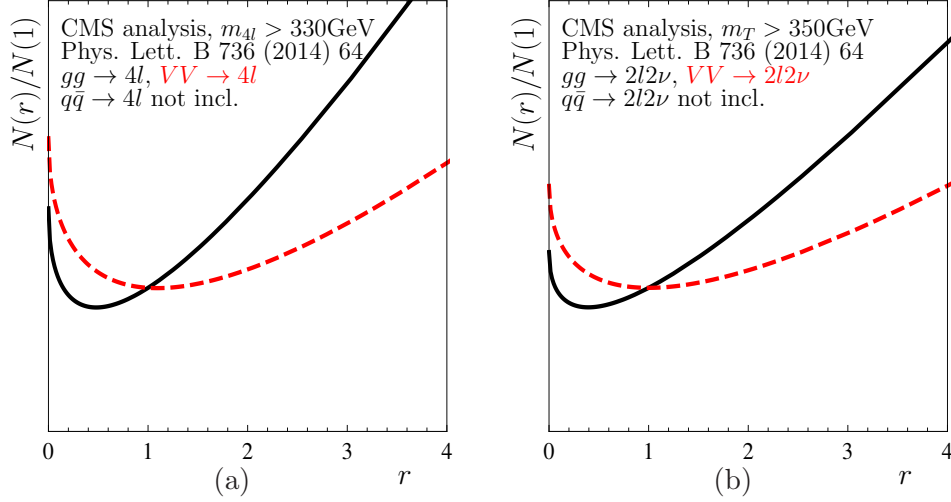


Figure 13: Normalised event rates $N(r)/N(1)$ as a function of r from the CMS analysis presented in Ref. [28] for the final states (a) $4l$ and (b) $2l2\nu$. The black solid curves show the gluon fusion production process, while the red dashed curves indicate the vector-boson fusion production process. In case (a) a likelihood discriminant characterizing the event topology and the cut on the invariant mass of the four leptons $m_{4l} > 330$ GeV was applied, in case (b) a transverse mass of $m_T > 350$ GeV and a missing energy of $E_T^{\text{miss}} > 100$ GeV was required. Since background events have been omitted in those plots, no scale is indicated on the y -axis. More details can be found in Ref. [28].

8 Effects of the heavy Higgs in a 2HDM

In this section we address interference effects of an on-shell heavy Higgs with the off-shell contributions of a SM-like light Higgs in the context of a 2-Higgs-Doublet model (2HDM). Studies for a singlet extension of the SM in gluon fusion at proton colliders were carried out in Refs. [66, 67], and significant interference effects dependent on the admixture of the singlet and the SM Higgs doublet were found. The authors of VBFNLO [68] studied the interference of an off-shell Higgs with a second Higgs in vector boson fusion at proton colliders. By an appropriate choice of the couplings the generic two Higgs model of VBFNLO can be used for the description of the light and heavy Higgs of a 2HDM. The scheme-dependence of parametrising the width for a heavy Higgs in the context of a Higgs portal scenario was discussed in Ref. [69].

The introduction of a second Higgs doublet is an obvious possibility for extending the SM Higgs sector, for reviews we refer to Refs. [70–75]. In our analysis we assume CP conservation in the Higgs sector and the absence of tree-level flavour-changing neutral currents. In this case the neutral Higgs sector consists of two CP-even Higgs bosons h and H with $m_h < m_H$ and one CP-odd Higgs boson A . One distinguishes four types of 2HDMs according to the structure of the Yukawa couplings. Before presenting results in the context of 2HDMs we shortly state our notation: The two Higgs doublets H_1 and H_2 acquire vacuum expectation values v_1 and v_2 , whose ratio is defined as $\tan\beta \equiv v_2/v_1$. The mixing angle rotating the neutral components H_1^0 and H_2^0 to mass eigenstates h and H is called α . Then the couplings

of h and H to the gauge bosons are given by

$$g_{hVV} = \sin(\beta - \alpha)g_{HVV}^{\text{SM}} \quad \text{and} \quad g_{HVV} = \cos(\beta - \alpha)g_{HVV}^{\text{SM}} \quad , \quad (16)$$

where g_{HVV}^{SM} denotes the coupling to the SM Higgs. For the light Higgs boson to be SM-like, $|\sin(\beta - \alpha)|$ has to be in the vicinity of one. As a consequence, the heavy Higgs H has heavily suppressed couplings to the gauge bosons in this case. In the following we study the deviations $\sin(\beta - \alpha) = \{0.95, 0.98, 0.99\}$ from one, the latter two providing a light Higgs boson h which is hardly discriminable from a SM Higgs boson at the LHC.

Since no Yukawa couplings are involved in our two production processes followed by $\{h, H\} \rightarrow VV^{(*)}$, the 2HDM type is only of relevance for the total widths Γ_h and Γ_H , which enter the Breit-Wigner propagators. The CP-odd state A does not couple to gauge bosons and therefore does not enter our calculation at lowest order in perturbation theory, when setting external fermion masses to zero. Our examples are all based on a type II 2HDM (Yukawa couplings as in the minimal supersymmetric standard model (MSSM)) with $\tan\beta = 1$. This guarantees stability of the Higgs potential and unitarity in gauge boson scattering, which we have checked with the help of 2HDMC [76]. We use the Higgs basis output of 2HDMC for the input file of MadGraph5_aMC@NLO. For the MSSM a rather heavy Higgs H and a CP-odd state A of similar mass imply that $\cos(\beta - \alpha)$ is close to zero, which reduces the sensitivity at a linear collider accordingly. In the MSSM values of $m_A \gtrsim 300$ GeV imply $\sin(\beta - \alpha) > 0.99$ for most of the parameter space. A heavy Higgs can then be observed through the process $e^+e^- \rightarrow Z^* \rightarrow AH$, which limits the detection to about $m_H \lesssim \sqrt{s}/2$. In Ref. [77] higher order corrections to the process $e^+e^- \rightarrow \nu\bar{\nu}H$ have been discussed, which can give rise to an upward shift of the detection limit in favourable regions of the parameter space.

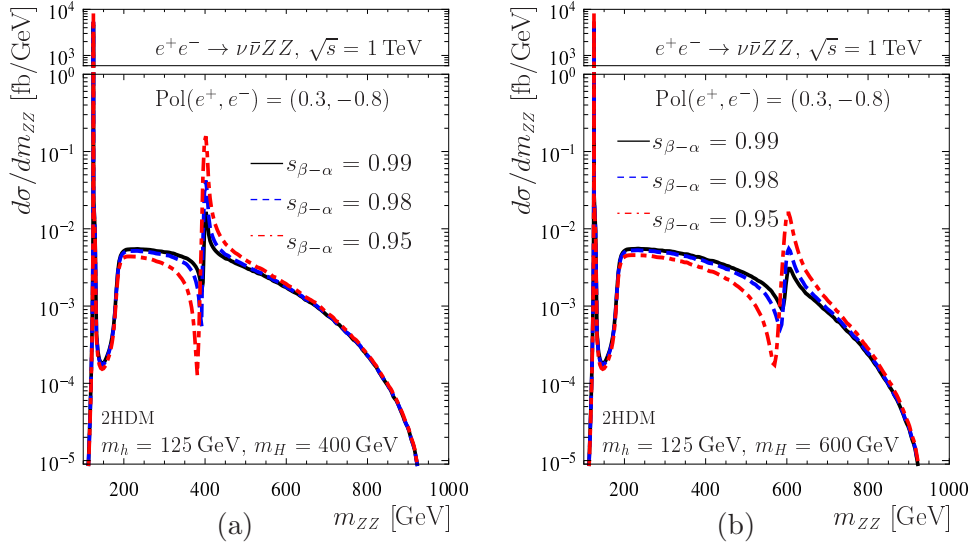


Figure 14: $d\sigma/dm_{ZZ}$ in fb/GeV as a function of m_{ZZ} in GeV for $\sqrt{s} = 1$ TeV and a fixed polarisation $\text{Pol}(e^+, e^-) = (0.3, -0.8)$ for the process $e^+e^- \rightarrow \nu\bar{\nu}\{h, H\} \rightarrow \nu\bar{\nu}ZZ$ in the context of a type II 2HDM with $\tan\beta = 1$ and three different values of $s_{\beta-\alpha} := \sin(\beta - \alpha)$ for the two mass scenarios (a) $m_H = 400$ GeV and (b) $m_H = 600$ GeV.

In the following we consider the process $e^+e^- \rightarrow \nu\bar{\nu}\{h, H\} \rightarrow \nu\bar{\nu}ZZ$ in the 2HDM and investigate the impact of the interference between the contributions of a heavy Higgs H and

a SM-like light Higgs h (with $m_h = 125$ GeV) on the sensitivity for detecting the heavy Higgs at a linear collider. We use $\sqrt{s} = 1$ TeV with a polarisation of $\text{Pol}(e^+, e^-) = (0.3, -0.8)$ and choose the two scenarios (a) $m_H = 400$ GeV, $m_A = 360$ GeV, $m_{H^\pm} = 440$ GeV and (b) $m_H = 600$ GeV, $m_A = 560$ GeV, $m_{H^\pm} = 640$ GeV, where for the latter case m_H lies beyond the kinematic reach of the HA pair production process. For $\sin(\beta - \alpha)$ we consider the three scenarios $\sin(\beta - \alpha) = \{0.95, 0.98, 0.99\}$. Fig. 14 shows the m_{ZZ} invariant mass distribution arising from this process. Below the threshold for on-shell production of the heavy Higgs H the distribution closely resembles the case of a SM Higgs at 125 GeV. The peak for the on-shell production of the light Higgs h and a continuum of off-shell contributions are clearly visible. At $m_{ZZ} = m_H$ the distribution shows a resonance-type behaviour with a significant interference contribution from the light Higgs. Since the heavy Higgs is only observable in $H \rightarrow VV$ for non-vanishing $\cos(\beta - \alpha)$, the effect on the m_{ZZ} distribution in the plot is largest for $\sin(\beta - \alpha) = 0.95$ and gets reduced as $\sin(\beta - \alpha)$ approaches unity. The shape of the m_{ZZ} distribution is furthermore affected by the total width Γ_H . The values for the heavy Higgs width Γ_H as obtained by 2HDMC are given in Tab. 8 for the scenarios considered here. For the heavy Higgs with mass $m_H = 600$ GeV the width exceeds 10 GeV, which results in a rather broad peak and $h - H$ interference structure. For invariant masses $m_{VV} > m_H$ the distribution receives off-shell contributions from both Higgs bosons. For high invariant masses the contributions of the two Higgs bosons add in such a way that they unitarize this process in the same way as the single contribution from a SM Higgs. Similar effects as the ones discussed here can also be expected at the LHC if the SM-like Higgs at 125 GeV is supplemented with a heavier neutral Higgs with suppressed couplings to gauge bosons (for a discussion of the vector boson fusion process at proton colliders with the help of VBFNLO see Ref. [68]).

Γ_H	$s_{\beta-\alpha} = 0.95$	$s_{\beta-\alpha} = 0.98$	$s_{\beta-\alpha} = 0.99$
$m_H = 400$ GeV	4.30 GeV	3.21 GeV	2.90 GeV
$m_H = 600$ GeV	19.1 GeV	16.4 GeV	16.1 GeV

Table 8: Heavy Higgs width Γ_H for the scenarios under consideration.

In order to discuss the prospects at the linear collider for this scenario in a more quantitative way, we now also incorporate background contributions into our analysis. Specifically we consider the process $e^+e^- \rightarrow \nu\bar{\nu}u\bar{u}d\bar{d}$, being a subprocess of $e^+e^- \rightarrow \nu\bar{\nu} + 4\text{jets}$ which includes $\{h, H\} \rightarrow ZZ^{(*)}/WW^{(*)} \rightarrow u\bar{u}d\bar{d}$. Similarly to Section 5 we cut on the transverse momentum of the 4jets and require it to be larger than 75 GeV. The result of our study can be found in Fig. 15. The narrow peak for $m_H = 400$ GeV can be seen by eye in all cases $\sin(\beta - \alpha) = \{0.95, 0.98, 0.99\}$. For $m_H = 600$ GeV again the peak broadens out. However, in all cases a side-band analysis of the background should have good prospects to reveal the heavy Higgs peak and the effect of the $h - H$ interference. The sensitivity for detecting an additional Higgs boson with suppressed couplings to gauge bosons at a linear collider can of course be enhanced by taking into account fermionic decays (and production modes where the additional Higgs boson is radiated off a fermion). We leave this topic for future work.

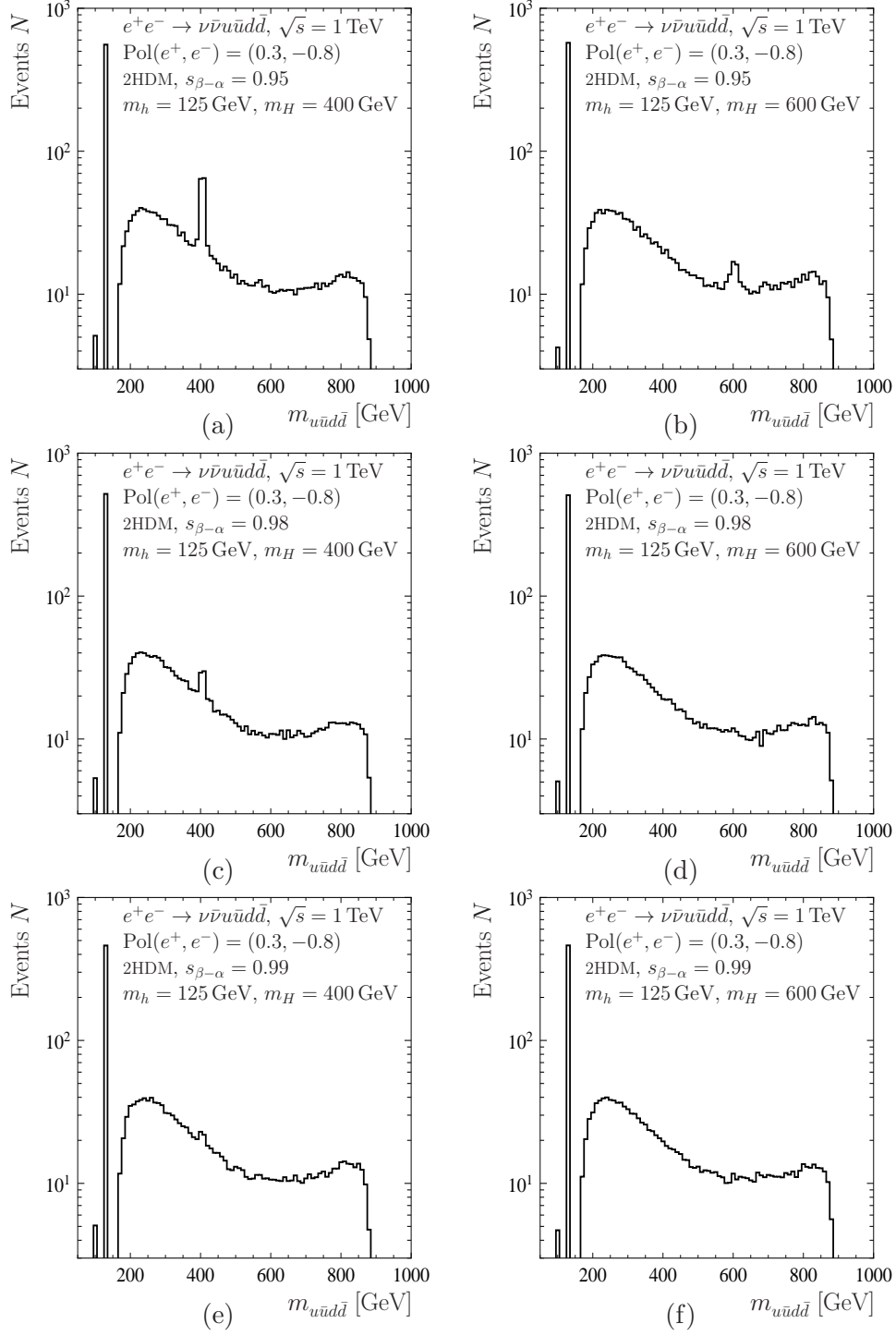


Figure 15: Event rates for $e^+e^- \rightarrow \nu\bar{\nu}u\bar{u}d\bar{d}$ for $\sqrt{s} = 1$ TeV and $\int \mathcal{L} dt = 500 \text{ fb}^{-1}$ after the cut $p_{T,4j} > 75$ GeV as a function of the invariant mass of the 4-jets $m_{u\bar{u}d\bar{d}}$ in the context of a type II 2HDM with $\tan\beta = 1$ for different values of (a,b) $s_{\beta-\alpha} := \sin(\beta - \alpha) = 0.95$; (c,d) $s_{\beta-\alpha} = 0.98$ and (e,f) $s_{\beta-\alpha} = 0.99$ and the two mass scenarios (a,c,e) $m_H = 400$ GeV and (b,d,f) $m_H = 600$ GeV.

9 Conclusions

We have investigated the impact of off-shell effects for Higgs production at a linear collider via the two production processes $e^+e^- \rightarrow ZH$ and $e^+e^- \rightarrow \nu\bar{\nu}H$ and the decay into a pair of gauge bosons, $H \rightarrow VV^{(*)}$ with $V \in \{Z, W\}$, for different cms energies and polarisations. The signal contributions involving a SM-like Higgs boson at 125 GeV have been compared with background yielding the same final state. We have performed numerical simulations of the full processes $e^+e^- \rightarrow 6$ fermions using `MadGraph5_aMC@NLO` and we have discussed the possible impact of initial state radiation and higher-order effects.

The fact that the mass of the observed Higgs boson of about 125 GeV is far below the threshold for on-shell W^+W^- and ZZ production has the consequence that the decay $H \rightarrow VV^*$ of an on-shell Higgs boson suffers from a significant phase-space suppression. This implies on the one hand that the partial width $H \rightarrow VV^*$, where H is on-shell, depends very sensitively on the precise numerical value of the Higgs-boson mass. On the other hand, contributions of an off-shell Higgs where VV are both on-shell are relatively large. This qualitative feature is reflected in our numerical analysis. The relative importance of contributions of an off-shell Higgs boson increases with increasing cms energy. For $\sqrt{s} > 500$ GeV those off-shell contributions to the total Higgs induced cross section are of $\mathcal{O}(10\%)$. The dependence on the precise numerical value of m_H is much diminished in the off-shell contributions as compared to the case of an on-shell Higgs.

Accordingly, for the extraction of Higgs couplings to gauge bosons from branching ratios of $H \rightarrow VV^*$ a very precise measurement of the Higgs-boson mass is needed, preferably to an accuracy of better than 100 MeV, and for higher cms energies it is important to take off-shell contributions into account. As expected, we find that at low cms energies \sqrt{s} , i.e. close to the production threshold, the effects of off-shell contributions are insignificant for the extraction of Higgs couplings. At higher \sqrt{s} , however, for an accurate determination of Higgs couplings the off-shell contributions need to be incorporated. Those contributions can furthermore be utilised to extract the Higgs to gauge boson couplings in different kinematical regimes, to check the destructive interference with the background or to set bounds on effective operators and test their kinetic dependences.

A particular focus of our analysis has been on the determination of the total width of the Higgs boson at a linear collider. We have investigated two aspects in this context. On the one hand, we have analysed to what extent the standard method at a linear collider, which is based on the Z recoil method providing absolute measurements of Higgs branching ratios in combination with an appropriate determination of a partial width, is affected by off-shell contributions. We have found that at low cms energies the effect of the off-shell contributions in $H \rightarrow VV^{(*)}$ is at the sub-permil level. At higher energies the off-shell effects can be somewhat larger and need to be properly taken into account and/or reduced by appropriate cuts. In this context our analysis adds to the motivation for performing the cross-section determination via the Z recoil method close to threshold, i.e. at about $\sqrt{s} = 250 - 350$ GeV, rather than at higher energies where the off-shell effects become relevant. On the other hand, we have investigated the constraints on the total width that can be obtained from a comparison of on-shell and off-shell contributions. At a linear collider those constraints are complementary to the determination of the Higgs width via the Z recoil method. However, the method based on the comparison of on-shell and off-shell contributions has several draw-backs. Besides relying heavily on theoretical assumptions, this method requires very high statistics

and is limited by the negative interference term. We therefore conclude that the standard method at a linear collider based on the Z recoil method is far superior for determining the Higgs width, both because of its model-independence and the much higher achievable precision. We have also discussed the corresponding method at the LHC and we have pointed out that the destructive interference contribution between the Higgs-induced contributions and the background will make it difficult to reach the sensitivity to the SM value of the width even for high statistics.

As an example of the relevance of off-shell effects in the context of an extended Higgs sector, we discussed the case of a 2-Higgs-Doublet model with a SM-like Higgs at 125 GeV and an additional heavier neutral CP-even Higgs boson with suppressed couplings to gauge bosons. We demonstrated the importance of the interference between off-shell contributions of the light Higgs and the on-shell contribution of the heavy Higgs. If the suppression of the couplings of the heavy Higgs boson to gauge bosons is not too strong, the $H \rightarrow VV^{(*)}$ channel can in this way lead to the detection of a heavy Higgs boson at a linear collider, even beyond the kinematic limit for producing a pair of heavy Higgs bosons, H and A .

The analyses performed in this paper can be improved in several respects, in particular regarding the inclusion of initial state radiation, beamstrahlung and higher-order effects. Concerning the latter, we demonstrated that they can be important, in particular in view of their dependence on the invariant mass of the two gauge bosons. Moreover future work might incorporate more sophisticated methods to identify intermediate particles or optimized cuts and statistical analyses to improve the sensitivity to off-shell effects and to discriminate between the various processes.

Acknowledgments

The authors thank Nikolas Kauer for helpful comments on the manuscript. The authors acknowledge support by the DFG through the SFB 676 “Particles, Strings and the Early Universe”. This research was supported in part by the European Commission through the “HiggsTools” Initial Training Network PITN-GA-2012-316704.

References

- [1] G. Aad *et al.* [ATLAS Collaboration], Phys. Lett. B **716** (2012) 1 [arXiv:1207.7214].
- [2] S. Chatrchyan *et al.* [CMS Collaboration], Phys. Lett. B **716** (2012) 30 [arXiv:1207.7235].
- [3] T. Behnke *et al.*, arXiv:1306.6327.
- [4] H. Baer *et al.*, arXiv:1306.6352.
- [5] C. Adolphsen *et al.*, arXiv:1306.6353.
- [6] C. Adolphsen *et al.*, arXiv:1306.6328.
- [7] T. Behnke *et al.*, arXiv:1306.6329.
- [8] G. Moortgat-Pick, H. Baer, M. Battaglia, G. Belanger, K. Fujii, J. Kalinowski, S. Heinemeyer and Y. Kiyo *et al.*, arXiv:1504.01726.

- [9] S. Dittmaier *et al.* [LHC Higgs Cross Section Working Group Coll.], arXiv:1101.0593.
- [10] S. Dittmaier *et al.* [LHC Higgs Cross Section Working Group Coll.], arXiv:1201.3084.
- [11] S. Heinemeyer *et al.* [LHC Higgs Cross Section Working Group Coll.], arXiv:1307.1347.
- [12] N. Kauer and G. Passarino, JHEP **1208** (2012) 116 [arXiv:1206.4803].
- [13] N. Kauer, Mod. Phys. Lett. A **28** (2013) 1330015 [arXiv:1305.2092].
- [14] N. Kauer, JHEP **1312** (2013) 082 [arXiv:1310.7011].
- [15] N. Kauer, arXiv:1502.02581.
- [16] E. W. N. Glover and J. J. van der Bij, Nucl. Phys. B **321** (1989) 561.
- [17] L. J. Dixon and M. S. Siu, Phys. Rev. Lett. **90** (2003) 252001 [hep-ph/0302233].
- [18] J. M. Campbell, R. K. Ellis and C. Williams, JHEP **1110** (2011) 005 [arXiv:1107.5569].
- [19] F. Caola and K. Melnikov, Phys. Rev. D **88** (2013) 054024 [arXiv:1307.4935].
- [20] J. M. Campbell, R. K. Ellis and C. Williams, JHEP **1404** (2014) 060 [arXiv:1311.3589].
- [21] J. M. Campbell, R. K. Ellis and C. Williams, Phys. Rev. D **89** (2014) 053011 [arXiv:1312.1628].
- [22] M. Chen, T. Cheng, J. S. Gainer, A. Korytov, K. T. Matchev, P. Milenovic, G. Mitselmakher and M. Park *et al.*, Phys. Rev. D **89** (2014) 034002 [arXiv:1310.1397].
- [23] I. Moulton and I. W. Stewart, JHEP **1409** (2014) 129 [arXiv:1405.5534].
- [24] J. M. Campbell, R. K. Ellis and C. Williams, PoS LL **2014** (2014) 008 [arXiv:1408.1723].
- [25] J. M. Campbell, R. K. Ellis, E. Furlan and R. Röntsch, Phys. Rev. D **90** (2014) 9, 093008 [arXiv:1409.1897].
- [26] J. M. Campbell and R. K. Ellis, JHEP **1504** (2015) 030 [arXiv:1502.02990].
- [27] CMS Collaboration [CMS Collaboration], CMS-PAS-HIG-14-002.
- [28] V. Khachatryan *et al.* [CMS Collaboration], Phys. Lett. B **736** (2014) 64 [arXiv:1405.3455].
- [29] ATLAS collaboration [ATLAS collaboration], ATLAS-CONF-2014-042.
- [30] J. S. Gainer, J. Lykken, K. T. Matchev, S. Mrenna and M. Park, Phys. Rev. D **91** (2015) 3, 035011 [arXiv:1403.4951].
- [31] M. Ghezzi, G. Passarino and S. Uccirati, PoS LL **2014** (2014) 072 [arXiv:1405.1925].
- [32] A. Azatov, C. Grojean, A. Paul and E. Salvioni, JETP Vol. 147 (3) (2015) [arXiv:1406.6338].

- [33] G. Cacciapaglia, A. Deandrea, G. Drieu La Rochelle and J. B. Flament, Phys. Rev. Lett. **113** (2014) 20, 201802 [arXiv:1406.1757].
- [34] M. Buschmann, D. Goncalves, S. Kuttimalai, M. Schönherr, F. Krauss and T. Plehn, JHEP **1502** (2015) 038 [arXiv:1410.5806].
- [35] H. Li, F. Richard, R. Poeschl and Z. Zhang, arXiv:0901.4893.
- [36] H. Li, arXiv:1007.2999.
- [37] H. Li *et al.* [ILD Design Study Group Collaboration], arXiv:1202.1439.
- [38] T. Han, Z. Liu and J. Sayre, Phys. Rev. D **89** (2014) 113006 [arXiv:1311.7155].
- [39] C. Dürig, K. Fujii, J. List and J. Tian, arXiv:1403.7734.
- [40] J. Alwall, R. Frederix, S. Frixione, V. Hirschi, F. Maltoni, O. Mattelaer, H.-S. Shao and T. Stelzer *et al.*, JHEP **1407** (2014) 079 [arXiv:1405.0301].
- [41] A. Denner, S. Dittmaier, M. Roth and D. Wackeroth, Nucl. Phys. B **560** (1999) 33 [hep-ph/9904472].
- [42] A. Denner and S. Dittmaier, Nucl. Phys. Proc. Suppl. **160** (2006) 22 [hep-ph/0605312].
- [43] S. Actis and G. Passarino, Nucl. Phys. B **777** (2007) 100 [hep-ph/0612124].
- [44] G. Passarino, C. Sturm and S. Uccirati, Nucl. Phys. B **834** (2010) 77 [arXiv:1001.3360].
- [45] S. Gorla, G. Passarino and D. Rosco, Nucl. Phys. B **864** (2012) 530 [arXiv:1112.5517].
- [46] J. Küblbeck, M. Böhm and A. Denner, Comput. Phys. Commun. **60** (1990) 165.
- [47] T. Hahn, Comput. Phys. Commun. **140** (2001) 418 [hep-ph/0012260].
- [48] T. Hahn and M. Perez-Victoria, Comput. Phys. Commun. **118** (1999) 153 [hep-ph/9807565].
- [49] E. Conte, B. Fuks and G. Serret, Comput. Phys. Commun. **184** (2013) 222 [arXiv:1206.1599].
- [50] V. D. Barger, T. Han and R. J. N. Phillips, Phys. Rev. D **39** (1989) 146.
- [51] A. Miyamoto, arXiv:1311.2248.
- [52] talks by T. Barklow and S. Watanuki at LCWS 2014, Belgrade, Serbia, <http://agenda.linearcollider.org/event/6389>
- [53] S. Kumar, P. Poulose and S. Sahoo, Phys. Rev. D **91** (2015) 7, 073016 [arXiv:1501.03283].
- [54] W. Kilian, T. Ohl, J. Reuter and M. Sekulla, Phys. Rev. D **91** (2015) 096007 [arXiv:1408.6207].
- [55] G. F. Giudice, C. Grojean, A. Pomarol and R. Rattazzi, JHEP **0706** (2007) 045 [hep-ph/0703164].

- [56] V. Barger, T. Han, P. Langacker, B. McElrath and P. Zerwas, Phys. Rev. D **67** (2003) 115001 [hep-ph/0301097].
- [57] R. Contino, C. Grojean, D. Pappadopulo, R. Rattazzi and A. Thamm, JHEP **1402** (2014) 006 [arXiv:1309.7038].
- [58] D. Barducci, H. Cai, S. De Curtis, F. J. Llanes-Estrada and S. Moretti, Phys. Rev. D **91** (2015) 9, 095013 [arXiv:1501.01830].
- [59] S. Dittmaier and M. Roth, Nucl. Phys. B **642** (2002) 307 [hep-ph/0206070].
- [60] E. Accomando, A. Denner and S. Pozzorini, JHEP **0703** (2007) 078 [hep-ph/0611289].
- [61] A. David *et al.* [LHC-HXSWG Collaboration], arXiv:1209.0040.
- [62] talk by G. Weiglein at the LHC-HXSWG 2 Meeting “Extension of kappa-framework”, CERN, Geneva, Switzerland, <https://indico.cern.ch/event/330239/>
- [63] C. Englert and M. Spannowsky, Phys. Rev. D **90** (2014) 053003 [arXiv:1405.0285].
- [64] C. Englert, Y. Soreq and M. Spannowsky, JHEP **1505** (2015) 145 [arXiv:1410.5440].
- [65] H. E. Logan, arXiv:1412.7577.
- [66] E. Maina, JHEP **1506** (2015) 004 [arXiv:1501.02139].
- [67] N. Kauer and C. O’Brien, arXiv:1502.04113.
- [68] J. Baglio, J. Bellm, F. Campanario, B. Feigl, J. Frank, T. Figy, M. Kerner and L. D. Ninh *et al.*, arXiv:1404.3940.
- [69] C. Englert, I. Low and M. Spannowsky, Phys. Rev. D **91** (2015) 7, 074029 [arXiv:1502.04678].
- [70] J. F. Gunion, H. E. Haber, G. L. Kane and S. Dawson, Front. Phys. **80** (2000) 1.
- [71] A. G. Akeroyd, Phys. Lett. B **377** (1996) 95 [hep-ph/9603445].
- [72] A. G. Akeroyd, J. Phys. G **24** (1998) 1983 [hep-ph/9803324].
- [73] M. Aoki, S. Kanemura, K. Tsumura and K. Yagyu, Phys. Rev. D **80** (2009) 015017 [arXiv:0902.4665].
- [74] G. C. Branco, P. M. Ferreira, L. Lavoura, M. N. Rebelo, M. Sher and J. P. Silva, Phys. Rept. **516** (2012) 1 [arXiv:1106.0034].
- [75] N. Craig and S. Thomas, JHEP **1211** (2012) 083 [arXiv:1207.4835].
- [76] D. Eriksson, J. Rathsman and O. Stål, Comput. Phys. Commun. **181** (2010) 189 [arXiv:0902.0851].
- [77] T. Hahn, S. Heinemeyer and G. Weiglein, Nucl. Phys. B **652** (2003) 229 [hep-ph/0211204].